POLITECNICO DI TORINO

Master's degree in Electrical Engineering

Master's Thesis

Effect of misalignment on a Tripolar Pad WPT System and Recognition Methods

Supervisor
prof. Paolo Guglielmi

Candidate
Damiano Zeferino

A.Y. 2022-2023

Contents

List of Tables 4

List of Figures 5

Introduction 11

1 Literature review 13
- 1.1 Classification of WPT systems . . . 13
- 1.2 Dynamic and static WPT . . . 14

2 Fundamentals of WPT systems for EV 17
- 2.1 Typical system configuration . . . 17
- 2.2 Main electrical parameters . . . 19
- 2.3 Compensation circuit . . . 23
- 2.4 Design choice for Pads and Coils . . . 25
  - 2.4.1 Single-phase systems . . . 26
  - 2.4.2 Multi-phase systems . . . 26

3 TPP Sistem Overview 29
- 3.1 TPP overlapped WPT . . . 29

4 Analytical model 33
- 4.1 Mutual inductance between circular windings . . . 34
  - 4.1.1 Two Coils System Analysis . . . 36
  - 4.1.2 Tripolar System Analysis . . . 37

5 Magnetic Analysis 41
- 5.1 Geometrical definition . . . 41
- 5.2 Coupling matrix calculation . . . 42
- 5.3 Perfect alignment and optimal α_{over} . . . 44
- 5.4 Misalignment effects . . . 47
  - 5.4.1 $\vec{x}$ axis misalignment . . . 49
  - 5.4.2 $\vec{y}$ axis misalignment . . . 51
  - 5.4.3 Mutual inductances in x-y misalignment . . . 53
  - 5.4.4 Rx pad rotation . . . 54
  - 5.4.5 x-y-λ misalignment . . . 56

6 Electrical Analisys 59
6.1 Independent coil system 62
6.1.1 Regular three-phase power supply 63
6.1.2 Single-coil supply 67
6.1.3 Practical issues 72
6.2 Delta connected topology 72
6.2.1 System simulation 74
6.2.2 Regular three-phase power supply 75
6.2.3 Opposing voltages supply 80

Conclusions 87

List of Tables

2.1 Capacitance values for primary and secondary circuits for different compensation topologies 25
6.1 Main parameters of the indipendent phases system simulation 64
6.2 Main parameters, delta connected system 76

List of Figures

1.1 Types of WPT systems 13
1.2 Typical position of an EV IPT system 15
1.3 Typical DWPT structures 16
2.1 Generic structure of a WPT system for EV charging 17
2.2 Bi-directional IPT system topology 18
2.3 Basic simplified circuit of a single-phase WPT system 19
2.4 Compensation topologies, single-phase WPT system 24
2.5 Typical single-phase coil structures for WPT 26
2.6 Typical multi-phase coil and pad structures for WPT systems 27
3.1 Tripolar *'pizza shape'* WPT 30
3.2 Linkage flux between mutually coupled coils 32
4.1 Simplified TPP-WPT geometry 33
4.2 Magnetic flux density induced by a current, Biot-Savart's law 35
4.3 Overlapped coils overview 39
5.1 Non-homologous and co-planar coupling coefficients trends for overlapping angle variations, perfect alignment case . . . 45
5.2 Non-homologous coupling coefficients trends for α_{over} and r_{coil} variations 46
5.3 Misalignment of Rx pad with respect to Tx in a vehicle . . . 48
5.4 $\vec{x}$ axis misalignment 49
5.5 Direct and cross-coupling inductances trends for $\vec{x}$-axis misalignment 50
5.6 $\vec{y}$ axis misalignment 51
5.7 Direct and cross-coupling inductances trends for $\vec{y}$-axis misalignment 52
5.8 Surface plot of direct mutual inductances for $\vec{x}-\vec{y}$ misalignment of the Rx pad, 3D and 2D view 53
5.9 Rx pad rotation 54

5.10 Direct and cross-coupling inductances trends for different angular positions of the receiving pad 55
5.11 Generic x-y-λ misalignment 56
5.12 Direct inductances trends for different angular positions of the receiving pad, generic x-y misalignment case 57
6.1 TPP-type WPT system with indipendent windings proposed by [10] 62
6.2 Circuit diagram of the WPT system with independent phases 63
6.3 Phase currents for misalignments along the Tx pad symmetry axes 65
6.4 66
6.5 Simplified Plecs model of WPT TPP system with independent phases for alternating power supply 68
6.6 Tx coils currents (top) and Rx (bottom) during 3-step test . 70
6.7 Phasor representation of homologous ($\vec{I_o}$, in red) and non-homologous ($\vec{I_n}$, in yellow) Rx-side currents in case of positive or negative mutual coupling. 71
6.8 Detail of the Tx current of the active phase (coil b) and the induced currents on the Rx side. 72
6.9 WPT circuit diagram with delta coil connection [4] 73
6.10 $YC - \Delta L$ circuit diagram 73
6.11 Equivalent circuit model with line and phase currents 74
6.12 Simulated circuit, regular three-phase power supply 76
6.13 Rx-side line currents for misalignments along symmetry axes, regular three-phase supply 77
6.14 Displacement map with Tx-Rx line currents, regular three-phase power supply 79
6.15 Line voltages phasor representation: regular three-phase supply (left) and opposing voltages supply (right) 80
6.16 Simulation diagram, power supply with opposing voltages . . 81
6.17 Line currents and voltages on Tx (left) and Rx (right) side of WPT system with delta connection 82
6.18 $\hat{I}_c$ and $\hat{I}_C$ trends for misalignments along the three symmetry axes 83
6.19 Line currents on Tx and Rx-side for misalignments along the three symmetry axes 84
6.20 Variation of the axis (in black) where null coil current is experienced, changing the non-fed coil (in red) 84

6.21 Non-fed coil currents for misalignments along $y = x$, $y = -x$ and $y = 0$ 86

Abstract

This Master's thesis work proposes an analytical study of the effects that misalignment causes in a wireless power transfer (WPT) system. WPT systems may become more practical charging solutions in the near future that will enable more frequent recharging, thus opening up the possibility of reducing the size of vehicle battery packs. Among the most important challenges to be faced, however, appear to be those of ensuring high transferable powers at efficiencies comparable to those of "wired" systems; in addition to the chosen geometry and electrical characteristics, misalignment is one of the factors that most degrades the performance of such systems: designing structures with high tolerance to misalignment and ensuring as much alignment as possible during energy transfer seem to be the two most important objectives in this regard. This thesis work proposes a simplified analytical model of a tripolar WPT system, through which a magnetic analysis is performed on the effects of misalignment between the two parts of the system. An algorithm based on Biot-Savart's law was used to calculate the magnetic couplings matrix for generic positions between the two pads; this matrix is then used in electrical simulations of the system, with the goal of analyzing the effects on the electrical quantities of the system due to the various possible misalignments. The main objective turns out to be to recognize the mutual position between the pads without using accessory systems, using only the electrical quantities easily measurable in the system.

Introduction

In the last decade, the development of electric cars has been driven primarily by the environmental issue, the need for the entire mobility and industrial sector to reduce energy consumption and related pollutant emissions.
The electrical transition, in particular, aims to increase the energy efficiency of many human activities, with the goal also of being able to use an increasing percentage of electricity from RES sources (wind, photovoltaic, etc.), which will become increasingly central to the energy strategies of all countries as the years go by, both for environmental and energy security issues.
Electric cars are actually not a recent idea; in fact, first prototypes of electric vehicles were already developed almost a century ago, but the technological limitations were such that this technology could not be developed properly.
With recent innovations in the areas of electrochemical storage systems, electric motors and power converters, it has been possible to secure a better perspective for this new mobility concept.
Other means of transport have long since relied on electricity for their operation, e.g. trams, trains, and there are other examples of electric vehicles for the so-called 'micro-mobility', e.g. logistical handling machines on construction sites, or the well-known golf karts etc., which, however, do not make a difference in terms of energy consumption and pollutant emissions.
There are many limitations and issues that still need to be resolved for e-mobility to become more widespread, and the main and most challenging ones are:

- Technology costs: due to the advanced technologies used, electric cars are significantly more expensive than their counterparts powered by ICE powertrains; in particular, the majority of the cost is caused by the battery storage system.

- Vehicle autonomy: this depends mainly on the technology used for the batteries. To date, the most widely used technology is lithium-ion cells, which, however, as already shown, are significantly more expensive than fuel, and have a significantly lower energy density. Compared to internal combustion engine (ICE) vehicles, electric vehicles traditionally have a shorter autonomy, and this is due to the difference in energy density between modern batteries and oil, or other fossil fuel sources. The energy density of standard oil is about 8200 Wh/kg, more than 10 times higher than the one of the current Li-Ion batteries, and still not comparable with respect to emerging battery technologies.[6]

- Capillarity of recharging infrastructures and speed of recharging: the presence of adequate infrastructures for recharging cars is a great issue for people to be enticed to make an investment in e-mobility; likewise, the speed of recharging vehicles is a limitation for buyers, as very long waiting times make this technology impractical for everyday life.

Many of these problems are already being resolved or alleviated; in general, the electric car will spread best when cost and practicality will make it fully equivalent to, if not better than, the internal combustion cars that still have the largest share of the market.
In this sense, the development of new recharging systems, with higher power transfer rates and high efficiencies, can make a difference: in particular, wireless recharging systems could be really useful if they maintain the characteristics just mentioned, and do not increase the total cost of the cars.

Chapter 1

Literature review

1.1 Classification of WPT systems

Since the second half of the 21st century, numerous experiments have been conducted on power transfer systems without the use of conductive cables connecting the source with the load, transferring power using only the air-gap between the two parts of the system. In general, WPT systems can be classified according to the technology they use: the main ones are inductive, capacitive, and microwave WPT (Fig.1.1) [9].

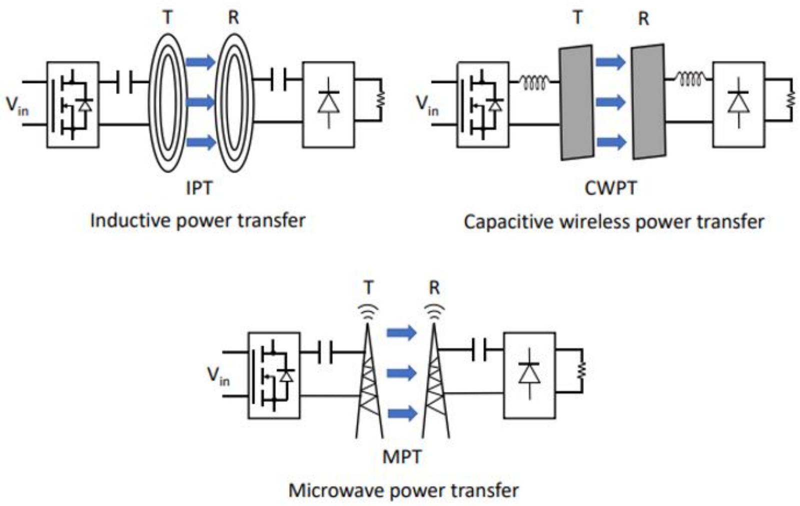

Figure 1.1. Types of WPT systems

Capacitive type systems (CWPT) involve the coupling of two conducting surfaces to form a capacitor, capable of transferring small amounts of power over equally small distances. The advantage of these systems is their size and cost [8]: for these reasons they are used for charging small instruments or in the medical field, in the case of implantable systems that aim to be minimally invasive.
Microwave systems (MPT), on the other hand, involve the transmission of energy in the form of electromagnetic waves, at frequencies in the order of radio frequencies, via a transmitting and a receiving antenna, which then filters and rectifies the signal appropriately, to feed the load downstream of the system. To date, these systems are not capable of transmitting large amounts of energy, and their main problem is that if both sides of the system are not in perfect resonance, the performance of the system degrades very quickly [9].
The IPT (inductive power transfer) systems are certainly the most commonly known, and the physical criterion on which they are based is used in many instruments in the industrial and domestic fields. Apart from their peculiarities, the basic structure is given by two coupled inductors, one receiving and one transmitting, between which power transfer takes place thanks to their magnetic coupling; the transmitting system generates a high-frequency magnetic flux ($80 - 100kHz$), which, on the basis of Faraday's law of magnetic induction, generates an induced voltage in the receiving system, and thus an induced current, which is suitably rectified and filtered to feed a load. Based on the same phenomenon also other kind of systems work, e.g. induction heating devices, in which a primary circuit generates an high-frequency magnetic field that induces a temperature rise in a conductive material due to the hysteresis of the material and the induced eddy currents.
IPT systems are the most suitable for automotive applications, as they can transfer larger amounts of power, and in practice are quite simple to implement, with the transmitter system on the ground and the receiver system fixed under the vehicle, transferring magnetic power through the air-gap between the two, as visible in Fig.1.2. [7]

1.2 Dynamic and static WPT

Academic research on automotive inductive WPT systems is mainly focusing on two types of systems, called *'Static power Charge'* and *'Dynamic*

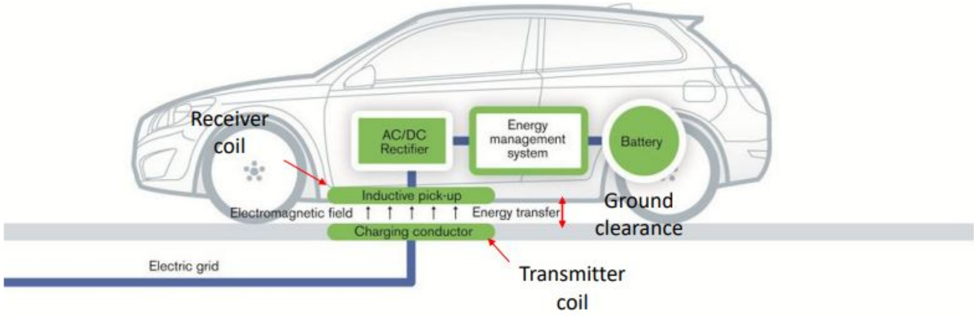

Figure 1.2. Typical position of an EV IPT system

power Charge'.
Static power charge consists on the transfer of power between two pads without any relative movement between the two. The main advantage of this type of system is that higher magnetic coupling can be achieved, limited only due to the air-gap between the two parts. The main challenge for the implementation of these systems is to achieve *"Ultra-Fast WPT"* [4]: manage the transfer of high powers ($> 100kW$) for ultra-fast charging of the battery pack. From the public transportation power line, the DC power supply can be derived to connect the high-frequency converters which feed the charging stations [4].
The operating principle of 'Dynamic power Charge' systems, on the other hand, is to have a structure placed on the ground that allows power to be transferred even while the vehicle is in motion, i.e. in the OLEV (On-line Electric Vehicle) phase. This charging method can in turn be divided into two types, depending on the type of transmitting structure used:

- *"Single Coil Track"*: In this version, the transmitter track is composed of a single inductor circuit, like a sort of track that transfers power to the receiver pad on the vehicle. The main problem with this type of system is the presence of only one converter on the transmitter side, which must have an oversized current rating in order to provide power for the simultaneous charging of vehicles. In addition, due to the structure of the transmitter 'track', there are large leakage fluxes that decrease the efficiency of the system.[4]

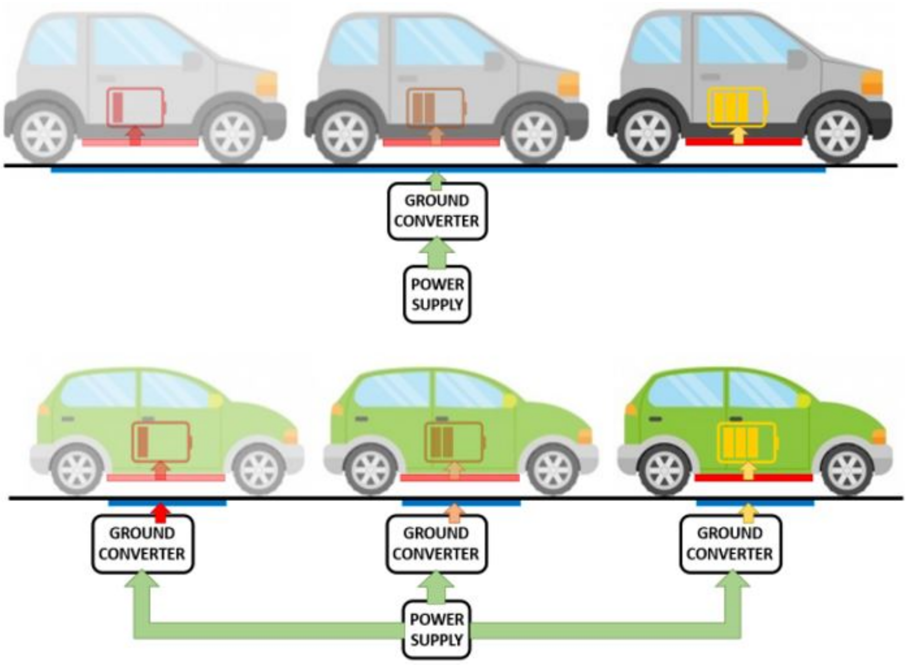

Figure 1.3. Typical DWPT structures

- *"Multi-Coil System"*: in order to overcome the problems of the previous system, an alternative solution is to provide a road route with a sequence of separate transmitting coils, powered by separate converters, which are in turn connected to the same power source. In this way, I do not need to oversize the ground-side converters, as each pad will be magnetically coupled to only one vehicle at a time; with such a structure, we can also ensure the maximum possible energy transfer to all vehicles.[4]

The downside of the dynamic charge is in any case performance; the reciprocal movement between the transmitter and receiver system does not guarantee a stable magnetic coupling between the two, generating a decrease in performance compared to corresponding static charging systems. Secondly, these systems are more complex and involve much higher investment costs, thus limiting their deployment.

Chapter 2

Fundamentals of WPT systems for EV

2.1 Typical system configuration

A typical inductive WPT system for EV charging purposes can be schematized as in the equivalent single-phase representation in Fig.2.1.

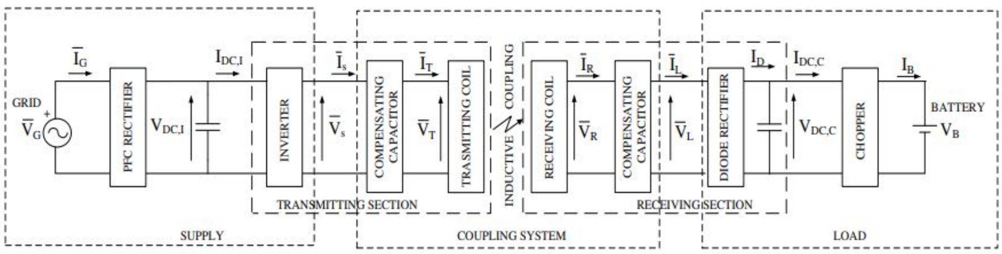

Figure 2.1. Generic structure of a WPT system for EV charging

The system consists of magnetically coupled windings that transmit power through a certain air-gap. The two pads, transmitter and receiver, may be composed by one or more coils, depending on the type of system used, and on both sides of the system there is usually a compensation circuit to minimize the effect of the inductive impedance of windings and maximize the power transfer capability.
On the transmitter side, the pad is powered by an inverter, which includes a PFC stage for power factor correction in the case of grid power supply, to

minimize the power absorbed. The inverter's task is to supply the transmitting coils with high-frequency voltages in order to generate variable magnetic fields that induce high-frequency voltages at the receiving coils. The induced voltages on the Rx pad side are then appropriately rectified by means of a stage that can be controlled or uncontrolled; in cascade with the rectifier, a possible DC-DC converter can be considered to adapt the output voltage to the load.
The choice of the right system topology is today a topic under investigation and depends on various factors, including the function of the system itself. In recent years in particular, with the increased popularity of RES, people have begun to talk about possible V2G functions for electric vehicles, with vehicles with electrochemical accumulators being able to exchange electrical energy bi-directionally with the power grid. This can be achieved by replacing the uncontrolled rectifier stage with a full bridge inverter [6], as shown in Fig.2.2.

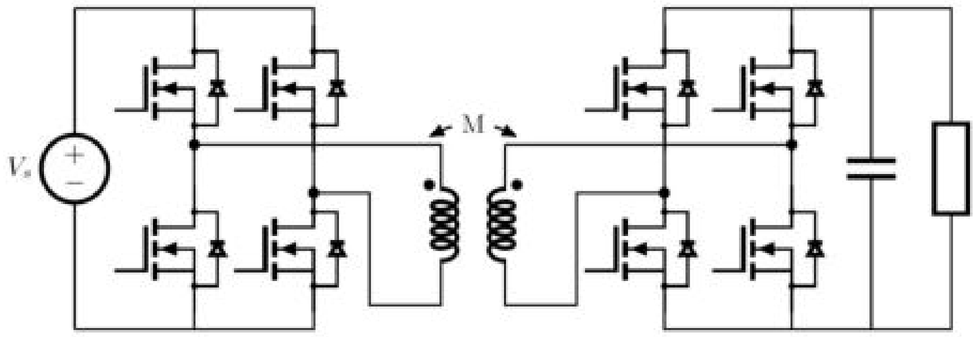

Figure 2.2. Bi-directional IPT system topology

In any case, one of the main objectives in making these systems simpler and more economical is undoubtedly to reduce the number of converters required for their operation, with consequent advantages also in terms of total system performance.

2.2 Main electrical parameters

Coupling coefficient

The most significant problem with WPT systems lies mainly in their physical attribute: they do not transmit power via conductive material, as in *"wired"* systems, nor are the two inductors magnetically coupled via a ferromagnetic core as in the case of capacitors. Power is transmitted only through air, which implies that the magnetic coupling between the two systems cannot be optimal.

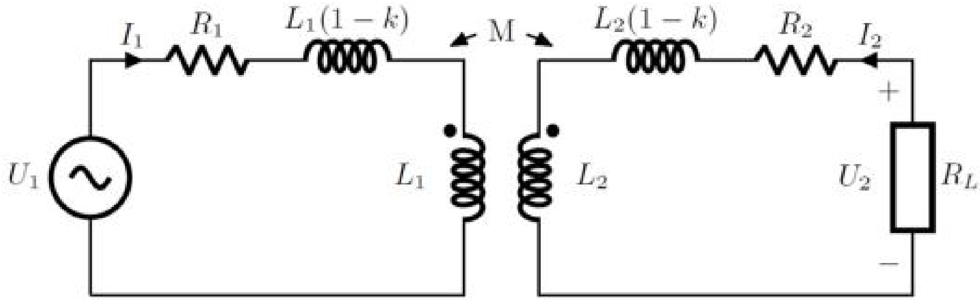

Figure 2.3. Basic simplified circuit of a single-phase WPT system

Considering the simplified schematic of an inductive WPT system in Fig.2.3, the coupling of the two inductors in the system can be represented via the mutual inductance M, but each of them also has a resistance, which dissipates power, and a self-inductance L_1 and L_2.
The presence of the air-gap causes high leakage fluxes, represented in the circuit as leakage inductances; the parameter indicating the degree of magnetic coupling between the two components of the system is called *coupling coefficient* k and is given by:

$$k = \frac{M}{\sqrt{L_1 \cdot L_2}} \tag{2.1}$$

To have positive power transfer between the two circuits, permitted values of k are $0 < k < 1$, where the unitary factor indicates perfect coupling between the two circuits, and a null one means complete decoupling.
Transformers are able to achieve coupling coefficients close to unity due to

the presence of the ferromagnetic core; in the case of inductive WPT systems, with magnetic fluxes concatenated in air, typical k-values are around $k \approx 0.2 - 0.4$.
In order to increase the coupling coefficient of the system as much as possible, it is necessary to increase the share of mutual inductance M with the same self-inductance of the coils: for this purpose, the choice of the right coil geometry of the system is crucial and can significantly improve the misalignment tolerance.

Mutual inductance and power transfer capability

Maximizing M is of crucial importance, both to increase power transfer capability and to reduce power losses, increasing the efficiency.
Considering the simplified system of Fig.2.3, I can define the maximum apparent transferable power as:

$$\bar{S}_{u2} = \frac{(j\omega M \bar{I}_{1ac})^2}{R_2 + j\omega L_2} \xrightarrow{R_2 \approx 0} \frac{\omega M^2 \bar{I}_{1ac}^2}{L_2} \tag{2.2}$$

The term in the numerator represents the induced voltage at the end of the receiving coil, while R_2 is the resistance of the secondary coil. The term $\frac{M^2}{L}$ is known as *power transfer capability*, i.e. the ability of the system to transfer power; it represents the coupling between the two systems, and does not depend on the electrical quantities, but only on its geometry: it must be optimized to limit flux leakage and increase M and consequently the coupling factor k. Since the transferable power depends quadratically on M, as the mutual inductance increases, the transferable power also increases.
For systems working at high frequencies, the inductive impedance of the coils limits the transferable power, which is why compensation networks are used. With series-series capacitive compensation, the simplest to represent in analytical relations, I will have that:

$$\bar{S}_{c2} = \frac{(j\omega M \bar{I}_{1ac})^2}{R_2 + [j\omega L_2 + \frac{1}{j\omega C}]} \tag{2.3}$$

At the resonance frequency ω_0, if the capacitance has been chosen appropriately, there will be perfect compensation of the coil inductance, and the system will be able to transfer the maximum possible power, given by:

$$P_{max} = \bar{S}_{c2} = \frac{(j\omega_0 M \bar{I}_{1ac})^2}{R_2 + [j\omega_0 L_2 + \frac{1}{j\omega_0 C}]} \approx \frac{\omega_0^2 M^2 \bar{I}_{1ac}^2}{R_2} = \frac{\omega_0 M^2 \bar{I}_{1ac}^2}{L_2} \cdot \frac{\omega_0 L_2}{R_2} = \\ = |\bar{S}_{u2}| \cdot q_S \tag{2.4}$$

The term q_S is called *secondary quality factor*, and it is recommended that it should have values no higher than 10, in order to have a system that is well controllable and to reduce its apparent power rating [5].
As can be seen from the equations, the factors that have the greatest impact on P_{max} are those with quadratic dependence, M and I_1: however, to increase the transferred power, it is more advisable to work on the mutual inductance rather than on the current, since increasing the primary current implies the use of larger converters and reactive elements, with higher temperature ratings, and thus greater economic expenditure.
A capacitive compensation network can also be used at the primary, with the aim of decreasing power ratings at the primary; in this way, two quality factors can thus be defined, for primary and secondary respectively:

$$q_P = \frac{\omega_0 L_1}{R_1} \qquad q_S = \frac{\omega_0 L_2}{R_2} \tag{2.5}$$

Using the coupling coefficient k I can rewrite the equation 2.2:

$$P_{max} = \frac{\omega_0 M^2 \bar{I}_{1ac}^2}{L_2} \cdot q_S = \omega_0 \cdot L_1 \cdot \bar{I}_{1ac}^2 \cdot k^2 \cdot q_S \tag{2.6}$$

where P_{max} is quadratically dependent on the factor k, and it is also proportional to the operating frequency chosen for the system.

Frequency choice and efficiency

The operating frequency of a WPT system is perhaps the most important parameter to choose at the design stage. Indeed, it has an impact on almost all the most important parameters considered for wireless power transfer systems.
It has already been shown through the relations previously presented for the power transfer in a compensated WPT system (2.2), that increasing the operating frequency of the system also increases the power that can

be transferred from it. The benefits of using high frequencies do not stop there; if we consider the reference single-phase model, with the secondary perfectly compensated, the efficiency of the system will be proportional to the chosen frequency, and will be:

$$\eta = \frac{P_2}{P_1} = \frac{\bar{S}_{u2} \cdot q_s q_p}{Q_1} = \frac{\omega_0 \cdot L_1 \cdot \bar{I}_{1ac}^2 \cdot k^2 \cdot q_S q_p}{Q_1} \tag{2.7}$$

By increasing the operative frequency, I can also reduce the size of reactive components of the compensation network: as will be discussed below, it can be seen from the relations in Tab.2.1 that, as a first approximation, in all capacitive compensation topologies the value of the required capacitances are inversely proportional to the term ω_0^2.
Increasing the frequency, however, has also negative effects, limiting its increase beyond certain limits:

- Increasing winding resistance due to skin effect and proximity effect
- Increasing switching losses
- Health Issues

The best way to overcome the first problem is to use Litz-type conductors; it is known that the penetration thickness of the current in a conductor is related to its frequency by the relationship:

$$\delta = \sqrt{\frac{2 \cdot \rho}{\omega \cdot \mu}} \tag{2.8}$$

it tends to decrease as the frequency increases. The Litz wire is composed by many conductors of small cross-sectional area and insulated from each other so that the penetration thickness is not less than the radius of the individual conductor strands.
As far as switching losses are concerned, the appropriate choice of power electronics, and thus of the kind of switch used, can limit the problem, ensuring that they have as little impact as possible on the total system performance.
Over the years in experiments on WPT systems, there has been a tendency to increase the operating frequency of the system from 20kHz to the current range of 75-90kHz: to date, the frequency used for this type of system is around 85kHz [1].

As far as the protection of people is concerned, there are constantly updated standards that impose precise exposure limits for these systems; on WPT systems for EV charging, the main reference standard is the ICNIRP for LFA (1 Hz-100 kHz) [1].

2.3 Compensation circuit

In an inductive WPT system, compensation of coil self-inductances is necessary mainly due to the high leakage fluxes present due to air coupling.
The effect of perfect compensation is precisely to make the impedance at both sides of the system equal to the phase resistance alone, thus putting phase voltages and currents in phase, minimizing the power rating of the system[8].
In systems with a coupling factor $k > 0.5$, such as a conventional ferromagnetic core transformer, the compensation capacitance should resonate with the leakage inductance. Whereas in an air-core system with $k < 0.5$, the compensation capacitance must resonate with the self-inductance to achieve a resistive impedance [6].
The most commonly used methods of compensation are those involving capacitors in series or in parallel, on both sides of the system: depending on the case, there are 4 basic structures of compensation, SS, SP, PS, and PP (Fig.2.4), with "S" and "P" indicating the position of the capacitors on the Tx and Rx sides. The values of the capacitances required to ensure resonance at both sides of the system are shown in Tab.2.1 [4].

SS topology

Series-to-series compensation is the simplest topology to implement in a WPT system. It involves two capacitors in series, one at the input of the Tx coil and the other at the output of the Rx. The compensation capacitance is chosen with the aim of canceling out the inductive reactance of the single coil, and depends both on the operating frequency of the system and the self-inductances of the coils.
With the series connection, the current flowing in the capacitor will be the same as the one flowing in the coils, which can make the capacitors vulnerable in case of high misalignment in the system, as currents would be very high and components could be damaged [6].

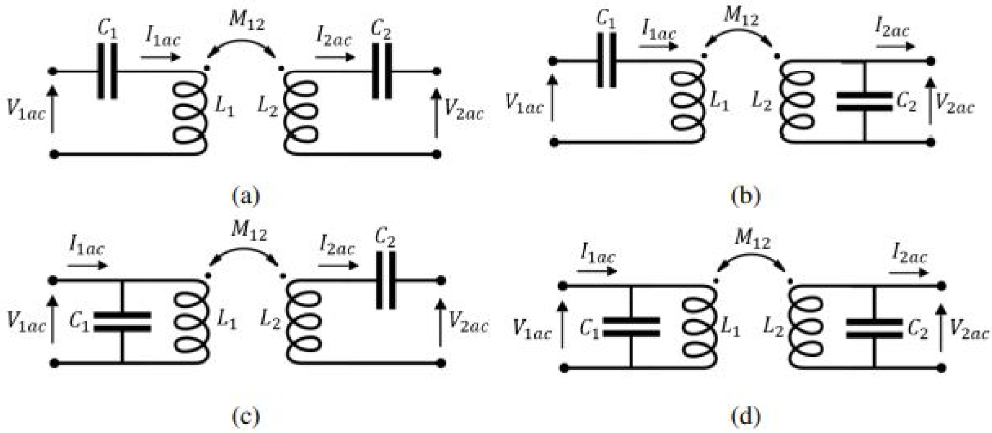

Figure 2.4. Compensation topologies, single-phase WPT system

Undoubtedly, the greatest advantage of this compensation topology is that the required capacitance value does not depend on either the load or the coupling of the system, so I will have a verified resonance condition in every possible situation.

SP topology

With SP compensation, the resonance capacitors are connected in series with the coils in the primary circuit, in parallel to the secondary. With the SP connection, in fact, the primary can be considered an equivalent current generator, the secondary a voltage generator, and this would allow for a stable voltage to the load downstream of the system.
As in the previous case, the main disadvantage of this topology is that at high misalignments the primary impedance becomes very low, thus leading to very high and potentially damaging currents. Another characteristic of this topology is the dependence of the compensation capacitance on the mutual inductance, which causes the loss of perfect resonance condition in case of misalignment.

PP e PS topologies

The PP and PS types are linked by the parallel compensation at the primary circuit, with the secondary connected in parallel or series, respectively.

In these topologies, the calculation of the resonating capacitance is more complex, since it depends on both the mutual and the downstream load. Furthermore, since the capacitors are connected in parallel on the Tx side, the power supply circuit must act as an equivalent current generator, in order to prevent overvoltages [1].

	Primary capacitance	Secondary capacitance
SS	$C_p = \frac{1}{\omega_0^2 \cdot L_p}$	$C_s = \frac{1}{\omega_0^2 \cdot L_s}$
SP	$C_p = \frac{1}{\omega_0^2 \cdot (L_p - \frac{M^2}{L_s})}$	$C_s = \frac{1}{\omega_0^2 \cdot L_s}$
PS	$C_p = \frac{L_p}{(\frac{\omega_0^2 M^2}{R_{load}})^2 + \omega_0^2 \cdot L_p^2}$	$C_s = \frac{1}{\omega_0^2 \cdot L_s}$
PP	$C_p = \frac{L_p - \frac{M^2}{L_s}}{(\frac{M^2 R_{load}}{L_s^2})^2 + \omega_0^2 (L_p - \frac{M^2}{L_s})^2}$	$C_s = \frac{1}{\omega_0^2 \cdot L_s}$

Table 2.1. Capacitance values for primary and secondary circuits for different compensation topologies

2.4 Design choice for Pads and Coils

There are many pad configurations in the literature, with well-known characteristics and peculiarities. The choice of the right coil and pad geometries is made according to various objectives:

- Increasing power transfer capacity;
- Maximise the mutual useful inductance, hence the coupling coefficient k, to reduce leakage fluxes during operation;
- Ensuring greater misalignment tolerance.

These objectives are not mutually exclusive; in fact, one of the major research efforts is to find the best configurations that make the system more efficient, flexible and power-dense.

2.4.1 Single-phase systems

The first system configurations to be tested in the academic field were single-phase circular coils (CP), rectangular coils (RP) and also double-D configuration (DDP), shown in Fig.2.5 [9].

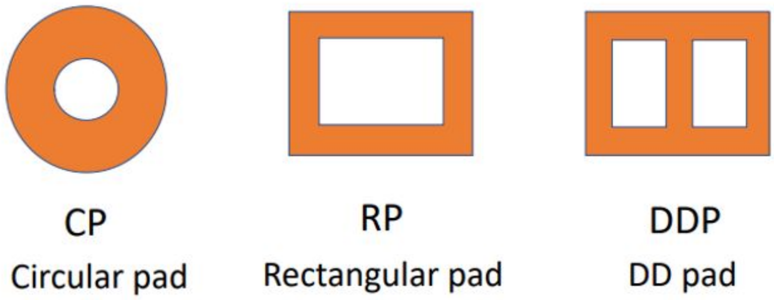

Figure 2.5. Typical single-phase coil structures for WPT

The main problem with these structures is that they suffer from a low coupling coefficient, which decreases dramatically as misalignment increases. Although the DDP structure allows greater tolerance to misalignment, the single-phase excitation generates a fixed magnetic field, and cannot be horizontally directed to compensate misalignments of the receiving pad [9].
Such easy-to-implement structures are used for charging small devices, such as wireless chargers for mobile phones.

2.4.2 Multi-phase systems

The advantage of using multi-phase structures is mainly that it is possible to direct the magnetic field at will, while adequately powering the transmitter pad. Double-D configurations with a quadrature coil (DDQP) and bipolar coil (BP) are based on the same criterion and have the advantage of being able to direct the magnetic field along the horizontal axis to compensate for Rx misalignments along it. In addition, by overlapping the coils, a complete magnetic decoupling between them can be achieved, making the system work as two separate single-phase systems [6] [9].

Given the results achieved with the addition of an additional phase,

Figure 2.6. Typical multi-phase coil and pad structures for WPT systems

three-phase systems have been proposed in recent years, with further investigation into systems with a higher phase number.
Structures such as TP1 (Fig.2.6) have a higher power density and tolerance to misalignment than the structures seen above, but the coils of the same pad suffer from reciprocal parasitic coupling that does not allow for optimized power transfer.
For this reason, structures with overlapping co-planar coils have been proposed, as in DDQP and BP, in order to eliminate mutual co-planar inductances and have three electrically independent phases. Variants of this structure can be distinguished on the basis of the external shape of the pad, among which is the so-called *"pizza shape"* type, which will be taken as a reference for the thesis work [2] [3].

Chapter 3

TPP Sistem Overview

3.1 TPP overlapped WPT

As already mentioned in the previous chapter, the system taken as reference for the analysis and studies in this thesis work is a WPT TPP system of the *"pizza shape"* type [3][2][4], developed within the PEIC laboratories of the Politecnico di Torino; this particular appellation is due to its characteristic shape: both the pads have a circular shape, with the individual windings arranged around and slightly overlapping each other.
The use of this characteristic geometry is possible because the system is designed to be used with a three-phase power supply so that both the transferable powers and the power density itself (kW/m^2) are high; the structure is also designed to be completely symmetrical on both sides, receiver (Rx) and transmitter (Tx): this makes its design simpler, limits leakage fluxes and potentially allows the system to be used in bi-directional mode (V2G) [4].

The most important feature of the system examined, however, is the overlap between the co-planar coils, which allows for improved efficiency and transferable power.
To introduce the concept, we can consider the system as six mutually coupled coils; all mutual induction coefficients between the elements of the system can be represented by a matrix $[M]_{6\times 6}$:

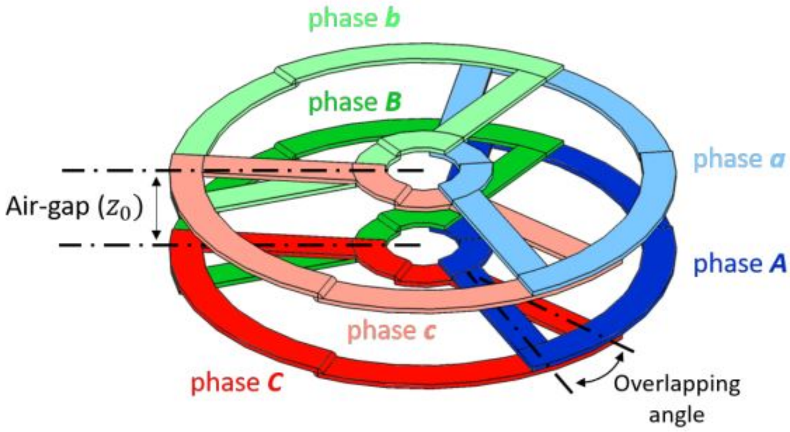

Figure 3.1. Tripolar *'pizza shape'* WPT

$$M_{ij} = \begin{bmatrix} a_{11} & a_{12} & a_{13} & a_{14} & a_{15} & a_{16} \\ a_{21} & a_{22} & a_{23} & a_{24} & a_{25} & a_{26} \\ a_{31} & a_{32} & a_{33} & a_{34} & a_{35} & a_{36} \\ a_{41} & a_{42} & a_{43} & a_{44} & a_{45} & a_{46} \\ a_{51} & a_{52} & a_{53} & a_{54} & a_{55} & a_{56} \\ a_{61} & a_{62} & a_{63} & a_{64} & a_{65} & a_{66} \end{bmatrix} \tag{3.1}$$

This matrix is symmetrical, since the mutual induction coefficients between two individual coils are unique, so it will be identical to its transpose. Furthermore, in the case of a coil structure that is symmetrical on both sides of the system, the elements of the main diagonal are all identical. The other elements, outside the main diagonal, represent the couplings between the coils in the system.
By appropriately overlapping the co-planar pads, it is possible to make the co-planar mutual inductance coefficients of the matrix negligible, and not only that: even the non-homologous coupling coefficients are, in the case of perfect alignment between the two pads of the system, completely negligible, making the matrix considerably simplified.
The matrix, with these adjustments, will take the following form:

$$M_{ij} = \begin{bmatrix} a_{11} & 0 & 0 & a_{14} & 0 & 0 \\ 0 & a_{22} & 0 & 0 & a_{25} & 0 \\ 0 & 0 & a_{33} & 0 & 0 & a_{36} \\ a_{41} & 0 & 0 & a_{44} & 0 & 0 \\ 0 & a_{52} & 0 & 0 & a_{55} & 0 \\ 0 & 0 & a_{63} & 0 & 0 & a_{66} \end{bmatrix} \tag{3.2}$$

Where the coefficients along the minor diagonals represent the homologous mutual inductances of the system, i.e. coupling coefficients between coils belonging to the same phases.
On an electrical level, the simplification implemented means that the electrical equations of the system are also simplified, and can be represented by the matrix equation 3.1:

$$\begin{bmatrix} \hat{V}_a \\ \hat{V}_b \\ \hat{V}_c \\ \hat{V}_A \\ \hat{V}_B \\ \hat{V}_C \end{bmatrix} = j\omega_0 \cdot \begin{bmatrix} 0 & 0 & 0 & -M_{aA} & 0 & 0 \\ 0 & 0 & 0 & 0 & -M_{bB} & 0 \\ 0 & 0 & 0 & 0 & 0 & -M_{cC} \\ M_{Aa} & 0 & 0 & 0 & 0 & 0 \\ 0 & M_{Bb} & 0 & 0 & 0 & 0 \\ 0 & 0 & M_{Cc} & 0 & 0 & 0 \end{bmatrix} \cdot \begin{bmatrix} \hat{I}_a \\ \hat{I}_b \\ \hat{I}_c \\ \hat{I}_A \\ \hat{I}_B \\ \hat{I}_C \end{bmatrix} \tag{3.3}$$

Where the voltages used are those supplying the coils, and the currents those flowing through them.
The system, under these conditions, can be treated as the union of three completely decoupled single-phase systems [2], with the homologous coupling coefficients identical under the assumption of a symmetrical system; the equations describing it will be:

$$\begin{cases} \hat{V}_{ph} = -j\omega_0 \cdot M\hat{I}_{PH} \\ \hat{V}_{PH} = j\omega_0 \cdot M\hat{I}_{ph} \end{cases} \tag{3.4}$$

And M turns out to be the only coupling factor to be considered for power transfer between the two pads.
The cancellation of coupling coefficients between overlapping coils can be explained in a simplified way by considering the case of two coils placed on parallel planes, at a distance between them fixed at z_0 (Fig.3.2).

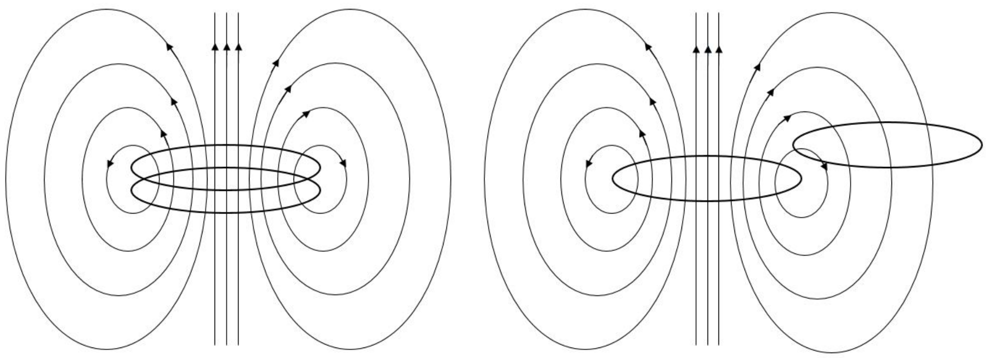

Figure 3.2. Linkage flux between mutually coupled coils

In the case in which the two loops are perfectly aligned, with the bottom loop active and the top loop completely passive, the flux generated by the current flowing in the first will be concatenated by the second in the positive $\vec{z}$ direction; in case of complete misalignment, on the other hand, the part of the flux that is concatenated by the passive loop does so in the opposite direction, in negative $\vec{z}$.
Thus, in the first case the mutual inductance between the two loops will be positive, in the second a negative mutual inductance will be experienced [5]. With a partial superposition of the two loops, it is therefore possible to make the mutual coupling between them perfectly null, canceling the flux in both directions.
These turn out to be ideal conditions for the system: in practical cases difficult to achieve; in the case of misalignment between the two pads, the coefficients simplified in 3.2 will not be negligible, so the coupling system will be more complex.
The main objectives of this thesis are to study these couplings as the misalignment between the two pads of the system varies, trying to identify the system misalignment during operations, and to be able to correct it, to maximize efficiency and the transferred power, as well as minimize leakage fluxes.

Chapter 4

Analytical model

In order to create an analytical model of the WPT system considered, it is necessary to consider a system with simplified geometry. This is because the real geometry is difficult to be represented with closed geometric formulas, due to its strong irregularity.
For this reason, the analysis will be performed by considering the coils of the system with a circular shape, as depicted in Fig.4.1

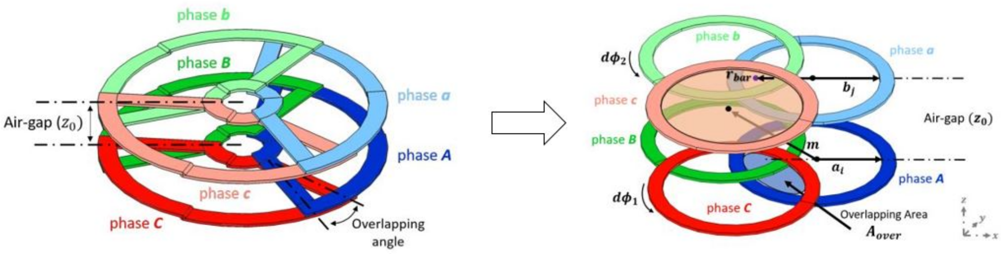

Figure 4.1. Simplified TPP-WPT geometry

Above all, this geometry makes it possible to simplify the calculation of the integrals of the relations used to calculate the magnetic couplings, as we shall see later in the chapter.

4.1 Mutual inductance between circular windings

In a system of coupled inductors, the calculation of the magnetic coupling coefficients is derived from well-known analytical formulas. The mutual inductance between two coupled inductors is calculated using the relation:

$$M_{12} = \frac{\vec{\Phi}_{12}}{\vec{I}_1} \tag{4.1}$$

In which $\vec{I}_1$ is the current flowing in the active inductor, while $\vec{\Phi}_{12}$ is the magnetic flux concatenated by the second inductor and produced by the first; this flux can in turn be calculated using the integral form of the corresponding Maxwell's law:

$$\vec{\Phi}_{12} = \oint_S \vec{B}_1 \cdot d\vec{S} \tag{4.2}$$

With $\vec{B}_1$ magnetic flux density generated by $\vec{I}_1$, and $\vec{S}$ the closed integration surface.
In the case of WPT systems, the magnetic induction is generated by current-carrying windings, so it is possible to use Biot-Savart's law for the calculation of $\vec{B}$, a special case of Laplace's much more general first formula on magnetic fields generated by electric currents; it states that a conductor, through which a current flows, generates a magnetic induction field given by:

$$\vec{B}(r) = \frac{\mu_0}{4 \cdot \pi} \cdot I \cdot \oint \frac{d\vec{l'} \cdot \Delta\vec{r}}{|\Delta\vec{r}|^3} \tag{4.3}$$

Where $\Delta\vec{r}$ identifies the position of the point P at which the field is calculated, while $d\vec{l'}$ is the infinitesimal stretch of conductor that generates it.

By combining the relationships just written, it becomes possible to calculate the mutual inductance between two coupled windings, which becomes:

$$M_{12} = M_{21} = \frac{\mu_0}{4 \cdot \pi} \cdot \int_{C_1} \int_{C_2} \frac{d\vec{l_1} \cdot d\vec{l_2}}{|\vec{R}|} \tag{4.4}$$

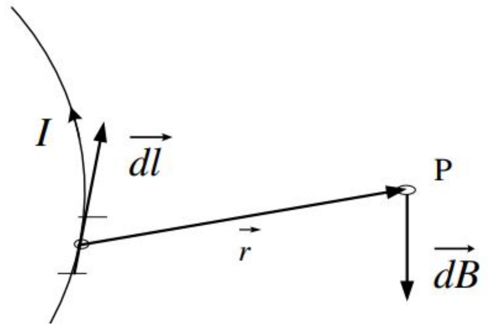

Figure 4.2. Magnetic flux density induced by a current, Biot-Savart's law

With $\vec{dl_1}$ and $\vec{dl_2}$ infinitesimal segments relating to the circular coils considered, while $|\vec{R}|$, representing the modulus of the vector joining the two infinitesimal segments $\vec{dl_1}$ and $\vec{dl_2}$ of the coils considered, at each step of integration.
The use of the simplified model presented in the introduction to the chapter has a crucial role for the development of this formula: the circular geometry of the coils allows a closed form to be developed, integrating the function in the circumferences of the coils C_1 and C_2.
Using the cylindrical coordinates, I can write the infinitesimal segment $\vec{dl}$ as a function of the coordinates of a generic point on the circumference:

$$dl = dx + dy = a \cdot (cos\phi - sen\phi)d\phi \tag{4.5}$$

where a is the radius of the winding, ϕ the angle. I can therefore rewrite the product $\vec{dl_1} \cdot \vec{dl_2}$ as:

$$dl_1 \cdot dl_2 = a \cdot b \cdot (cos(\phi_1 - \phi_2) - sen(\phi_1 - \phi_2))d\phi_1 \cdot d\phi_2 \tag{4.6}$$

a and b are the radii of the two windings, while ϕ_1 and ϕ_2 are the angles required to define the cylindrical coordinates [4]. At this point, the integral formula for calculating the mutual inductance between two circular windings can be modified to its final form:

$$M_{ij} = \frac{\mu_0}{4 \cdot \pi} \cdot \int_0^{2\pi} \int_0^{2\pi} \frac{a \cdot b \cdot [cos(\phi_1 - \phi_2) - sen(\phi_1 - \phi_2)]d\phi_1 \cdot d\phi_2}{|\vec{R}|} \tag{4.7}$$

Chosen the radii a, b of the two coils, the only element that remains to be evaluated is $|\vec{R}|$; however, it varies depending on the kind of structure and the reference system, so it is necessary to carry out a more in-depth analysis in this regard. In particular, starting from the simple case of two mutually coupled coils, the right relations for calculating $|\vec{R}|$ in the more complex case of the tripolar system under consideration will be derived later.

4.1.1 Two Coils System Analysis

Consider the case of two perfectly parallel windings in the axis $\vec{z}$, with their centers aligned; let us take as reference for the system the axes $\vec{x}\vec{y}$ passing through the center of the lower coil, while the upper coil, placed at a distance z_0, has its own reference axes $\vec{x}'\vec{y}'$; the distance $|\vec{R}|$ between two generic points of the two circumferences can be calculated as:

$$|\vec{R}| = \sqrt{\Delta x^2 + \Delta y^2 + \Delta z^2} = \sqrt{{z_0}^2 + [acos\phi_1 - bcos\phi_2]^2 + [asen\phi_1 - bsen\phi_2]^2} = \\ = \sqrt{{z_0}^2 + a^2 + b^2 - 2abcos(\phi_1 - \phi_2)} \tag{4.8}$$

In the case of coils with multiple windings placed side by side, the formula can be adapted by modifying the relations describing the radii a and b to represent the generic winding:

$$\begin{aligned} a_i &= a_0 + (i-1) \cdot d_{s_1} \\ b_j &= b_0 + (j-1) \cdot d_{s_2} \end{aligned} \tag{4.9}$$

with $d_{s_{1,2}}$ diameters of the conductors, a_i and b_j radii of the coils considered, i and j representing the number of coils, while a_o and b_o are the maximum radii of the windings of the two windings [4].
The calculation of the coupling coefficients will then become:

$$M_{tot} = \sum_{i=1}^{N_{s_1}} \sum_{j=1}^{N_{s_2}} M_{12_{ij}} \tag{4.10}$$

It is possible to consider a simplified version in which the loops are ideally overlapping and concentric: in that case, the total mutual inductance of 4.1.1 is given by the product of that of the individual loop by the total number considered.
In the case of non-aligned coils, in order to calculate the distance $|\vec{R}|$ between two generic points of the two coils, the misalignment must be taken

into account: it consists on the displacement of the $\vec{x}'\vec{y}'$ references with respect to the $\vec{x}\vec{y}$ one, with the axes that in this first analysis can be considered respectively parallel.
The new parameters to be considered will be $|\vec{m}|$, the modulus of the vector joining the centres of the circumferences, and α the angle between $\vec{x}$ and the projection of the vector $\vec{m}$ onto the plane $\vec{x}\vec{y}$. In this way, I will be able to write:

$$\begin{aligned} |\vec{R}_{ij}| &= \sqrt{{z_0}^2 + [mcos\alpha + a_i cos\phi_1 - b_j cos\phi_2]^2 + [msen\alpha + a_i sen\phi_1 - b_j sen\phi_2]^2} = \\ &= \sqrt{{z_0}^2 + a^2 + b^2 - 2abcos(\phi_1 - \phi_2)} \end{aligned} \tag{4.11}$$

It should be noted that in the simplified case of only two mutually coupled circular windings, the parameter α is irrelevant since once m is fixed, all the possible positioning points of the upper winding will guarantee the same magnetic coupling with the counterpart.
Its definition, as well as that of the two Cartesian references, is however really important for the study of more complex cases, with more windings to be considered as in the case of the tripolar WPT under consideration.

4.1.2 Tripolar System Analysis

The TPP system under study has a geometry that is certainly more complex than the simple case of two coupled coils, but we can still start from the relations previously found to derive those useful here.
The simplified tripolar system to be parameterized is composed, as already known, by three circular windings for each pad, perfectly equidistant from each other and with the same radius r_{coil}. We can therefore consider a coplanar coil system with reference axes $\vec{x}\vec{y}$, in which the origin of the axes also corresponds to the center of gravity of the tripolar system.
The distance between the centers of the individual coils and the center of gravity of the respective pad is the same for all of them and is indicated by the parameter r_{bar}, while the axes on which the centers lie are half-lines starting from the origin and displaced by 120° mechanically between them. For each pad, I can therefore define 3 fixed angles, with respect to the axis $\vec{y}$, which allow to calculate the Cartesian coordinates of the centers of the coils:

$$\begin{cases} \beta_{a,A} = 0 \\ \beta_{b,B} = \frac{2}{3}\pi \\ \beta_{c,C} = -\frac{2}{3}\pi \end{cases} \tag{4.12}$$

With these data, it is possible to calculate the modulus of the generic $\vec{R}$ vector joining two points belonging to coil of the two pads, with the formula:

$$\begin{aligned} &|\vec{R}_{ij}| = \sqrt{\Delta x^2 + \Delta y^2 + \Delta z^2} \\ &\Delta x = mcos\alpha + r_{bar}cos(\beta_i + \frac{\pi}{2}) + r_{coil}cos(\Phi_2) - r_{bar}sen(\beta_j + \frac{\pi}{2}) - r_{coil}sen\Phi_1 \\ &\Delta y = msen\alpha + r_{bar}sen(\beta_i + \frac{\pi}{2}) + r_{coil}sen(\Phi_2) - r_{bar}sen(\beta_j + \frac{\pi}{2}) - r_{coil}sen\Phi_1 \\ &\Delta z = z_0 \end{aligned} \tag{4.13}$$

where i, j are reference indices for the coils considered. It is also possible to parameterize a possible rotation of the receiving pad with respect to the transmitter: this rotation consists of the rotation of the reference system $\vec{x'}\vec{y'}$ of the receiving pad, with the active elements belonging to it moving in solidarity with the relative reference system. For this reason, we can introduce the angular parameter λ, which represents the angle between the $\vec{x'}$ axis of the receiver and the fixed reference $\vec{x}$.
The equations for calculating $\vec{R}$ will be adapted as follows:

$$\begin{aligned} &\Delta x = mcos\alpha + r_{bar}cos(\beta_i + \frac{\pi}{2} - \lambda) + r_{coil}cos(\Phi_2 - \lambda) - r_{bar}sen(\beta_j + \frac{\pi}{2}) - r_{coil}sen\Phi_1 \\ &\Delta y = msen\alpha + r_{bar}sen(\beta_i + \frac{\pi}{2} - \lambda) + r_{coil}sen(\Phi_2 - \lambda) - r_{bar}sen(\beta_j + \frac{\pi}{2}) - r_{coil}sen\Phi_1 \\ &\Delta z = z_0 \end{aligned} \tag{4.14}$$

The relations found will be further adapted in case of coupling between co-planar windings, with the necessary adjustments. The final goal is to have only one equation, through which it is possible to calculate the totality of the magnetic couplings, and thus all the coefficients of the coupling matrix.

Overlapping angle

As we know, in order to make parasitic couplings between non-homologous coils negligible, the coils of the same pad are overlapped by an angle α_{over}. This angle is directly related to r_{bar} and the radius of the coils r_{coil}, and if considered as a parameter of the system, it is possible to choose its optimal value by studying the trend of co-planar couplings with respect to its variation.

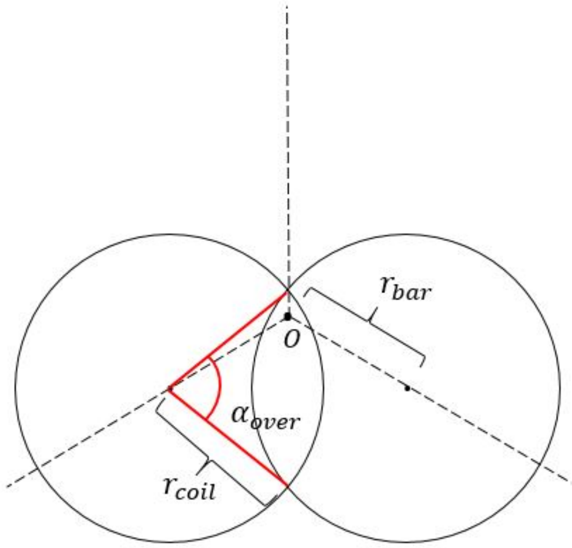

Figure 4.3. Overlapped coils overview

Consider the tripolar system with the coils displaced by 120 mechanical degrees between them; as r_{bar} changes, the co-planar coils will reciprocally approach or recede, which may lead to partial overlap between them.
It is possible to calculate r_{bar} as a function of the angle of overlap between two coils and their radius, with the relation:

$$r_{bar} = \frac{r_{coil} \cdot cos(\frac{\alpha_{over}}{2})}{sen(\frac{\beta}{2})} \tag{4.15}$$

where β is the angular distance between the two circumferences, thus known for the geometry of the system, i.e. $\beta = \frac{2}{3}\pi$.
This relation will be very useful to implement the calculation of the coupling

coefficients via MatLab for the system under consideration: knowing the value of, α_{over} which minimizes the co-planar couplings, I consequently also know the radius r_{bar}, hence the dimensions of the optimized system.
From the information on the overlapping angle between the coils, another useful quantity can be derived, the overlap area between the two co-planar couplings:

$$A_{over} = r_{coil}^2 \cdot (\alpha_{over} - 2 \cdot sen\alpha_{over} \cdot cos\alpha_{over}) \tag{4.16}$$

From this relationship, it can be deduced that for a hypothetical overlapping angle of 180° ($\alpha_{over} = \pi$), the area of the coil that is overlapped will be the total area of the coil $\pi \cdot r_{coil}^2$.

Chapter 5

Magnetic Analysis

5.1 Geometrical definition

The complete magnetic model of the system can be defined through the matrix $[M]_{6x6}$ of the magnetic couplings related to the coils composing it. The aim is to be able to define it for any reciprocal position between the two pads, so that the effects of misalignment on the coupling coefficients can be analyzed.
To do this, the well-known Matlab numerical calculation software was used, in which an algorithm was developed to calculate the coefficients of $[M]$, giving as input all the geometrical parameters of the system and the mutual position between pads, but also between coils belonging to the same subsystem (Tx-Rx).
The angles $\beta_{a,b,c}$ and $\beta_{A,B,C}$ are considered as constants since the angular position of the coils, with respect to the reference system to which they belong, is considered fixed. The first parameters required for the geometric definition of the system are r_{coil} and α_{over}; through the radius of the coils and the β angle it is indeed possible to calculate r_{bar} but also A_{over}, as seen in 4.15 and 4.16 respectively.
The radius of the individual coils was chosen on the basis of the limits imposed for the WPT system taken as reference, i.e. maximum dimensions of 85x85x7.5 cm. In an approximate way, it is possible to write the maximum dimensions x_{max} and y_{max} as a function of the radius r_{coil} only, considering the hypothesis of α_{over} null, and circumferences of the coils simply tangent to each other:

$$x_{max} = 2 \cdot r_{bar} \cdot sin(\frac{\pi}{3}) + 2 \cdot r_{coil}$$
$$y_{max} = 2 \cdot r_{bar} \cdot cos(\frac{\pi}{3}) + 2 \cdot r_{coil} \tag{5.1}$$

With α_{over} not explicitly appearing in the equation, but already considered as r_{bar} is dependent on it. Having set the geometric constraints, a suitable radius value that allows these constraints to be met is $r_{coil} = 20cm$, and will be the one used for the simulations.

5.2 Coupling matrix calculation

Having known the parameters defining the geometry of the system, what is needed to calculate the coupling coefficients through the algorithm are the relative position parameters between the pads.
Knowing the exact position of the center of gravity O' of the pad Rx with respect to Tx, uniquely determined by the coordinates (x_{pos}, y_{pos}, z_0), it is possible to determine the two cylindrical coordinates of the position of Rx on the plane $\vec{x} - \vec{y}$, namely m and the angle α, with the following relations:

$$m = \sqrt{x_{pos}^2 + y_{pos}^2} \qquad \alpha = sin^{-1}(\frac{y_{pos}}{m}) \qquad \alpha = cos^{-1}(\frac{x_{pos}}{m}) \tag{5.2}$$

Note, however, that using only one of the relations for the calculation of α would not allow the exact angle to be determined: this is because, as is well known, for each value of the sine and cosine functions there are always two corresponding angles, and not just one. By using both, however, this ambiguity is completely resolved.
To overcome this issue, the strategy used was to exploit the signs of the coordinates provided as input: in this way, by using a *if - elseif* type structure for comparing the signs, we can choose which of the two relations of 5.2 is the most suitable for calculation. In particular:

- if $x_{pos} > 0 \wedge \text{y}_{pos} > 0 \rightarrow \alpha = sin^{-1}(\frac{y_{pos}}{m})$
- if $x_{pos} < 0 \wedge \text{y}_{pos} > 0 \rightarrow \alpha = cos^{-1}(\frac{y_{pos}}{m})$
- if $x_{pos} < 0 \wedge \text{y}_{pos} < 0 \rightarrow \alpha = sin^{-1}(\frac{-y_{pos}}{m}) + \pi$

- if $x_{pos} > 0 \wedge y_{pos} < 0 \rightarrow \alpha = sin^{-1}(\frac{y_{pos}}{m})$

The conditions for the cases of $k\frac{\pi}{2}$ angles are also included:

- if $x_{pos} > 0 \wedge \mathrm{y}_{pos} = 0 \rightarrow \alpha = 0$

- if $x_{pos} = 0 \wedge \mathrm{y}_{pos} > 0 \rightarrow \alpha = \frac{\pi}{2}$

- if $x_{pos} < 0 \wedge \mathrm{y}_{pos} = 0 \rightarrow \alpha = \pi$

- if $x_{pos} = 0 \wedge \mathrm{y}_{pos} < 0 \rightarrow \alpha = \frac{3}{2}\pi$

Knowing the two cylindrical parameters, it is only necessary to know the angle of rotation of the receiving pad, referred to as λ, in order to have all the parameters required to calculate all the coupling matrix coefficients, with the general equation already identified:

$$M_{ij} = \frac{\mu_0}{4 \cdot \pi} \cdot \int_0^{2\pi} \int_0^{2\pi} \frac{a \cdot b \cdot [cos(\phi_1 - \phi_2) - sen(\phi_1 - \phi_2)] d\phi_1 \cdot d\phi_2}{|\vec{R}|} \tag{5.3}$$

With $|\vec{R}|$ distance between two generic points of the two windings i, j taken into consideration, which can be calculated with the known parameters via the equations 4.1.2.
It is possible to use the same formula to calculate all the coefficients of the matrix, and this can be done by changing the value of the geometric parameters of the system while keeping the equations identical. The equations are adapted as follows:

- For the co-planar coupling terms, $\Delta z \approx 0$ and also the terms $m, \lambda = 0$ are considered negligible;

- For the self-inductance terms, the same criterion is used as for co-planar couplings, with $\Delta z \approx 0$ and $m, \lambda = 0$, but in addition, we have also that $\beta_i = \beta_j$: the self-inductances can be calculated as the mutual inductance between two identical and concentric windings, placed at almost zero distance from each other;

- For non co-planar mutual inductances, $z_0 = 50cm$ is considered.

It can be noticed that, for the calculation of the self-inductance of individual coils, the equation 5.2 is used as if it were a co-planar mutual inductance between two perfectly overlapped coils [4].
Formally, if the mutual inductance M_{ab} between two coils is defined as the ratio between the flux linkage of coil b and the current $\vec{I_a}$ that generated it, similarly the self-inductance L of a single coil is defined as the ratio between the total flux produced by it and the current flowing through it:

$$L_i = \frac{\vec{\Phi}_i}{\vec{I_i}} \tag{5.4}$$

It was decided to use the dimension $z = 2.5cm$ for the calculation of all self-inductances, since in accordance with the definition made above, it can represent the real thickness of a coil used in the system.

5.3 Perfect alignment and optimal α_{over}

In case of perfect alignment, given the symmetries of the system, the mutual inductance coefficients between co-planar coils will be of equal value, as will be the mutual inductances between non-homologous coils (Tx-Rx); this aspect simplifies a lot the research for the ideal angle α_{over} that minimizes the parasitic coupling coefficients, since it is possible to study the trend of only two coefficients as the overlap between the windings varies: one represents the co-planar ones, the other the non co-planar ones; the results of the analytical study of this trend are shown in Fig.5.1.

The trends have been reported for an angle variation of $[0 - \pi]$. As can be seen, mutual inductances in both cases increase while the angle increases: for small angles they will have negative values, due to the fact that the windings would in that case concatenate the source flux with negative direction.
The range of α_{over} in which parasitic couplings are minimized is:

$$76° < \alpha_{over} < 81° \tag{5.5}$$

where the two extremes are the values that minimize non co-planar and co-planar coefficients respectively.
As nominal value for the simulations, it was chosen an angle equal to $\alpha_{over} = 79°$, from which r_{bar} is derived, allowing to calculate the magnetic coupling

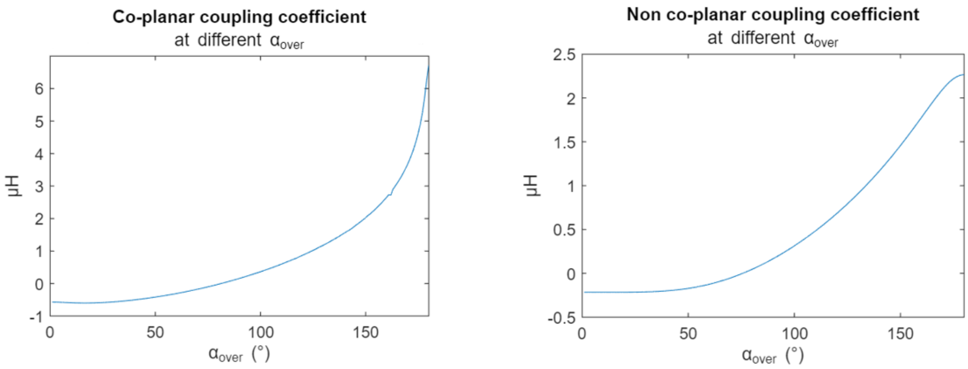

Figure 5.1. Non-homologous and co-planar coupling coefficients trends for overlapping angle variations, perfect alignment case

matrix of the system in case of perfect alignment and maximum decoupling between the phases:

$$M_{ij} = \begin{bmatrix} 6.728 & -0.038 & -0.038 & 2.265 & 0.034 & 0.034 \\ -0.038 & 6.728 & -0.038 & 0.034 & 2.265 & 0.034 \\ -0.038 & -0.038 & 6.728 & 0.034 & 0.034 & 2.265 \\ 2.265 & 0.034 & 0.034 & 6.728 & -0.038 & -0.038 \\ 0.034 & 2.265 & 0.034 & -0.038 & 6.728 & -0.038 \\ 0.034 & 0.034 & 2.265 & -0.038 & -0.038 & 6.728 \end{bmatrix} \cdot \mu H \tag{5.6}$$

As can be seen, the value of parasitic couplings is two orders of magnitude lower than the self-inductances and homologous ones, and therefore negligible in this configuration.
It can be observed that, in the case of $\alpha_{over} = \pi$, the co-planar coupling coefficients will be equal to the self-inductance of the coils, while the cross-coupling coefficients will be equal to the direct mutual inductance, i.e. the maximum coupling achievable by two non co-planar coils of the system.
A very interesting behavior can be noticed regarding the overlapping angle definition. By plotting the trend of the mutual couplings between coils as α_{over} and also r_{coil} change, as depicted in Fig.5.2, for circular coils the optimal overlapping angle to minimize co-planar couplings is basically fixed:

it is equivalent to $\alpha_{over} \approx 81°$ as seen above, and is equivalent to a misalignment between the two coils of approximately 76% of the coil radius, as already found by [5]. For non co-planar inductances, on the other hand, for the same distance z_0 between the two coils, there is no fixed value, but different optimal angles as the coil radius vary.

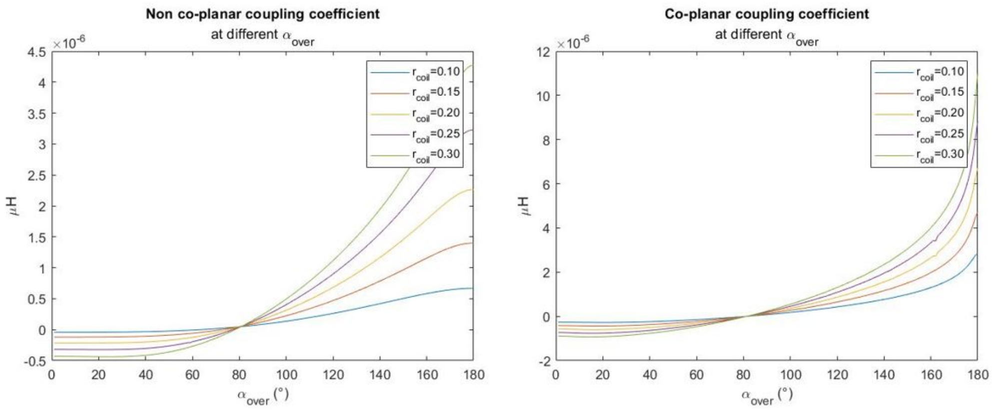

Figure 5.2. Non-homologous coupling coefficients trends for α_{over} and r_{coil} variations

It is also possible to see two other aspects of the system through its coupling matrix:

- [M] is a symmetrical matrix, as each pair of coils is linked by the same flux linkage;

- The optimum point of cross-coupling inductances, both co-planar and non co-planar, is not equal since the latter is influenced by the distance z_0 between the windings of different pads [4]; however, their values are not so distant from each other.

Assuming negligible parasitic couplings between phases, the simplified matrix will have the same structure as that seen in 3.2:

$$M_{ij} = \begin{bmatrix} 6.728 & 0 & 0 & 2.265 & 0 & 0 \\ 0 & 6.728 & 0 & 0 & 2.265 & 0 \\ 0 & 0 & 6.728 & 0 & 0 & 2.265 \\ 2.265 & 0 & 0 & 6.728 & 0 & 0 \\ 0 & 2.265 & 0 & 0 & 6.728 & 0 \\ 0 & 0 & 2.265 & 0 & 0 & 6.728 \end{bmatrix} \cdot \mu H \tag{5.7}$$

In real-life cases, however, perfect alignment between the two pads of the charging system is an ideal set-up that is difficult to achieve: the relative displacement between the two pads makes the couplings between the different phases no longer negligible, and also causes the value of the mutual homologous inductances to change, with a consequent effect on the transferable power, and not only that.

5.4 Misalignment effects

Misalignment, as already mentioned, is a real condition in the system, as in practical cases the system is never perfectly aligned. It can take various forms:

- $\vec{x}$-axis misalignment: typically due to the driver's lack of accuracy in positioning the vehicle due to his limited viewpoint, i.e. from the driving position; can be resolved almost completely if the vehicle location where the WPT system is located is marked by vertical boundary lines.

- $\vec{y}$-axis misalignment: also due to the driver's inaccuracy due to his limited viewpoint; it is the easiest to correct, as it does not require maneuvering.

- Rotation of the receiving pad with respect to the transmitting pad: this situation can also be avoided by the use of delimiting lines.

The case of non-parallel pads, with a variable $\vec{z}$ distance between them, has not been considered in the analysis performed: it is assumed that this kind of situation is already avoided with a correct fixation of Tx to the ground and a correct positioning of the Rx pad in the vehicle underbody.
With the right measures, it is possible to limit such misalignments, but

not always completely eliminate them. In the following chapter, the effects that these displacements have on the magnetic couplings will be studied, evaluating the three basic situations described above, as well as possible combinations.

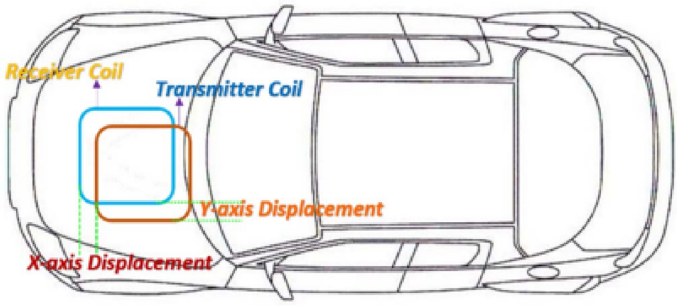

Figure 5.3. Misalignment of Rx pad with respect to Tx in a vehicle

5.4.1 $\vec{x}$ axis misalignment

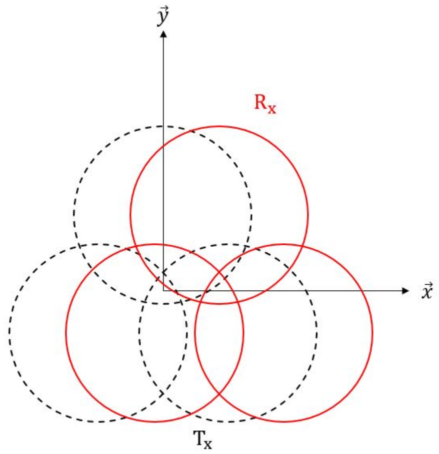

Figure 5.4. $\vec{x}$ axis misalignment

Given the structure and characteristics of the individual pads, we can use the analytical formulas previously found. Given the structure of the pads and their size, it is realistic to expect a maximum misalignment in the horizontal axis between them of $\pm 20cm$.
From the Matlab code, the trends of the coupling coefficients were extrapolated for horizontal misalignment changes, as visible in the plots in Fig.5.5.

It can be seen from the graph on the left that the non-homologous inductances, in the case of misalignment along the $\vec{x}$ axis, do not assume different values at all, but some of them have the same trend: this occurs due to symmetries generated during movement, such that the following equalities will occur:

$$\begin{cases} M_{aC} = M_{bA} \\ M_{aB} = M_{cA} \end{cases} \tag{5.8}$$

and since $[M]_{6x6}$ is symmetrical, the same will apply to the reciprocal coefficients.
All the direct mutual inductances, on the other hand, have the same trend, as can be seen in the second plot of Fig.5.5: this is because, in absence of receiver pad rotation, the misalignment will result in a displacement of the

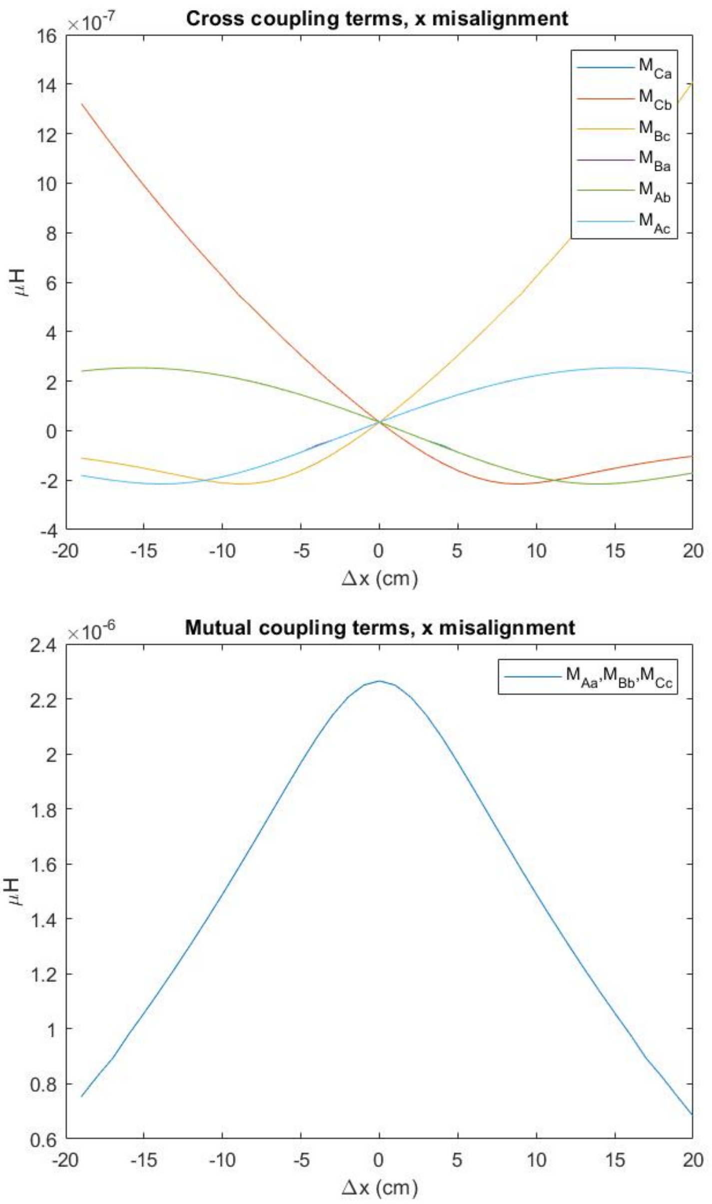

Figure 5.5. Direct and cross-coupling inductances trends for $\vec{x}$-axis misalignment

$\vec{x'}\,\vec{y'}$ reference, but the axes remain parallel to the fixed reference system; thus, the relative position between all the homologous coils is the same.

5.4.2 $\vec{y}$ axis misalignment

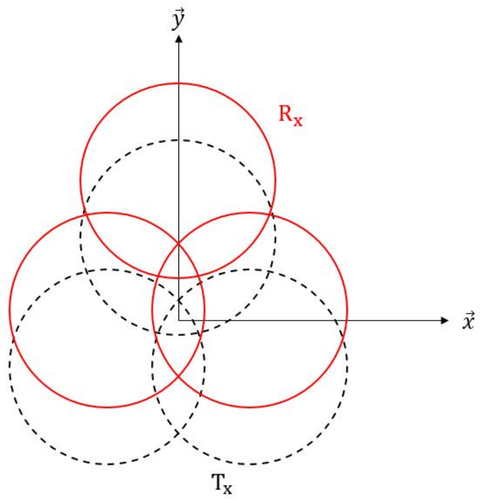

Figure 5.6. $\vec{y}$ axis misalignment

To study the trend of the coupling coefficients for $\vec{y}$-axis misalignments, we use the same extremes as before, with a maximum displacement limit of $\pm 20cm$. The results are plotted in Fig.5.7.

In this case, the displacement along the $\vec{y}$ axis generates more symmetries than in the previous case, and these equalities can be found:

$$\begin{cases} M_{bA} = M_{cA} \\ M_{aB} = M_{aC} \\ M_{cB} = M_{bC} \end{cases} \tag{5.9}$$

All the cross-coupling coefficients assume only 3 different values, and this happens because $\vec{y}$ represents an axis of symmetry for the Tx system; moving along the other two axes of symmetry of the system I would have similar conditions, but with different mutualities.
As it was expected, the direct mutual inductances have the same trend, for the same reason previously exposed.

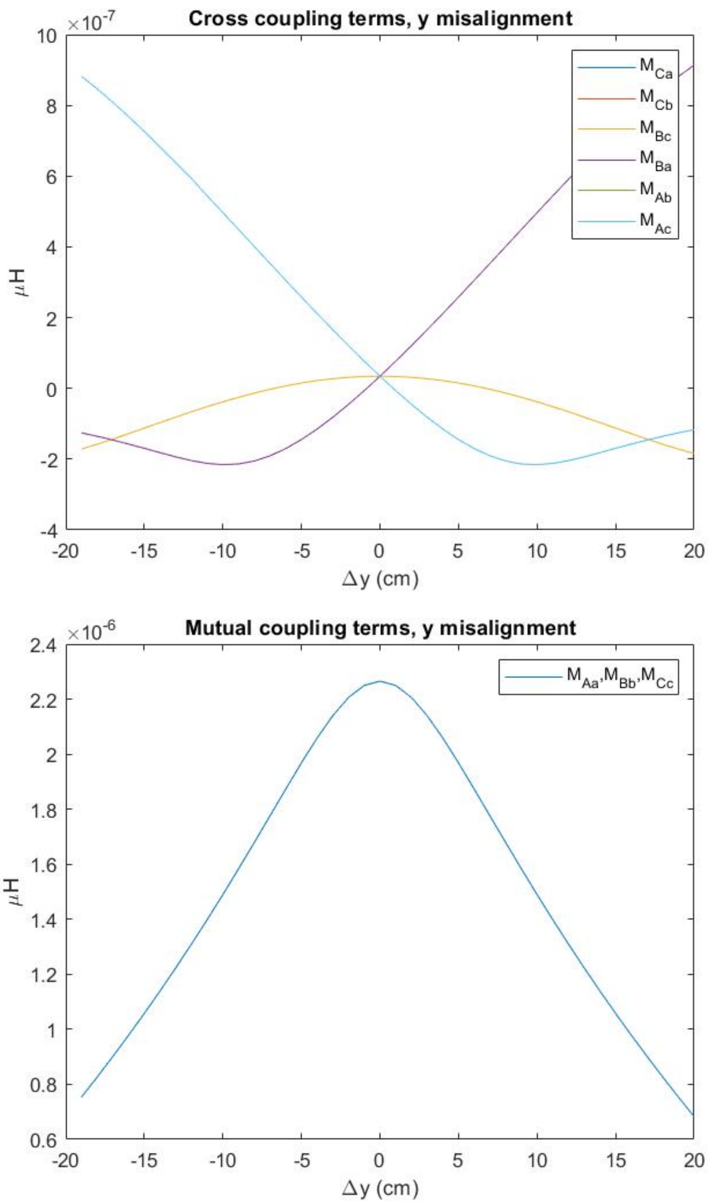

Figure 5.7. Direct and cross-coupling inductances trends for $\vec{y}$-axis misalignment

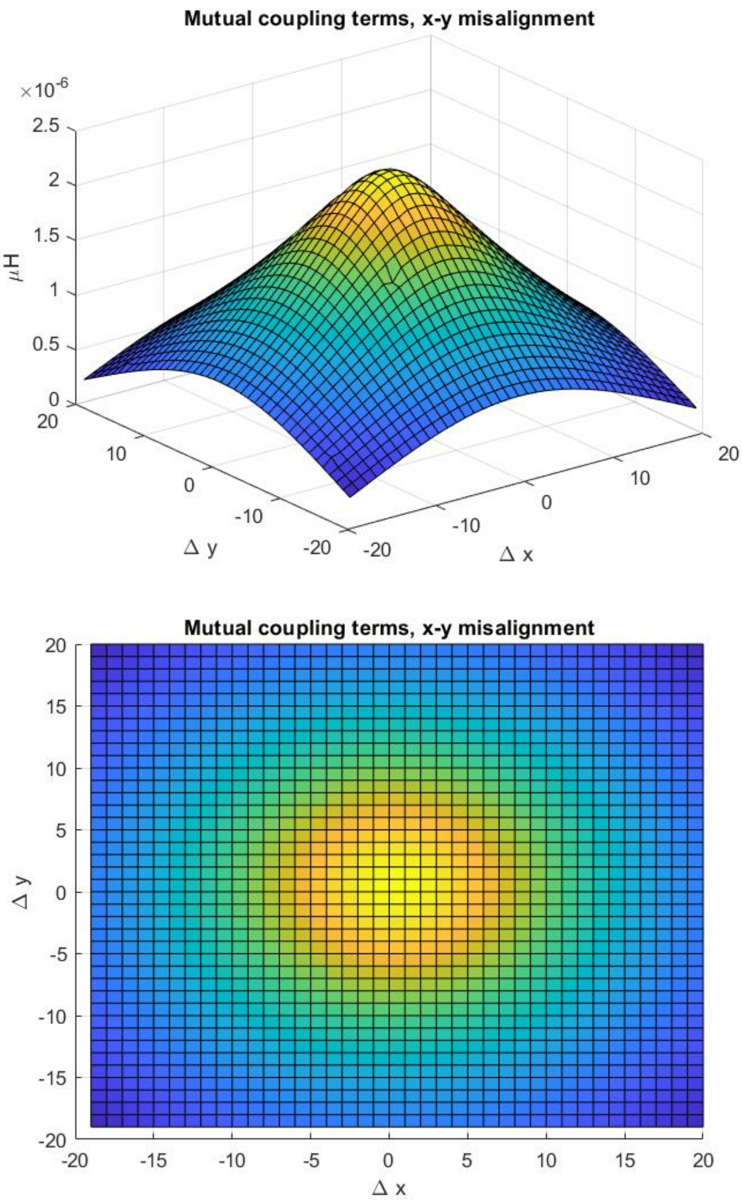

Figure 5.8. Surface plot of direct mutual inductances for $\vec{x}-\vec{y}$ misalignment of the Rx pad, 3D and 2D view

5.4.3 Mutual inductances in x-y misalignment

Consider the case of generic misalignment in $\vec{x}-\vec{y}$ of the receiving pad, without rotation of the pad itself; it is possible to draw a three-dimensional plot of the magnetic couplings, for all the possible displacement of Rx.

Fig.5.8 shows the plot of homologous mutual inductances as the position of Rx changes, with the same displacement limits assumed in the previous cases.
From the plots, it is possible to notice that the value of direct inductances is equal along concentric circles, with respect to the center of Tx, i.e. the point of perfect alignment between the two pads.
With the analytical notation used in the previous chapters, we can therefore state that direct mutual inductances vary as m varies, and decrease as this radius increases since the receiving system tends to move away from the transmitting one.

5.4.4 Rx pad rotation

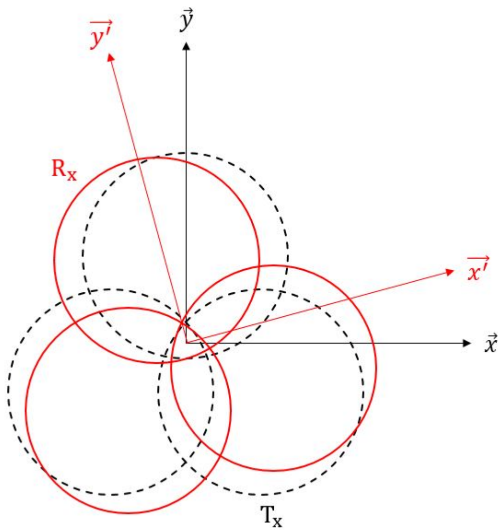

Figure 5.9. Rx pad rotation

The rotation of the receiver was simulated under the assumption of perfect alignment of the two Tx-Rx centers of gravity. The simulation results are shown in the graphs in Fig.5.10

Also in this case there are several equalities between cross-coupling coefficients, due to the symmetries generated in the system by the mere rotation

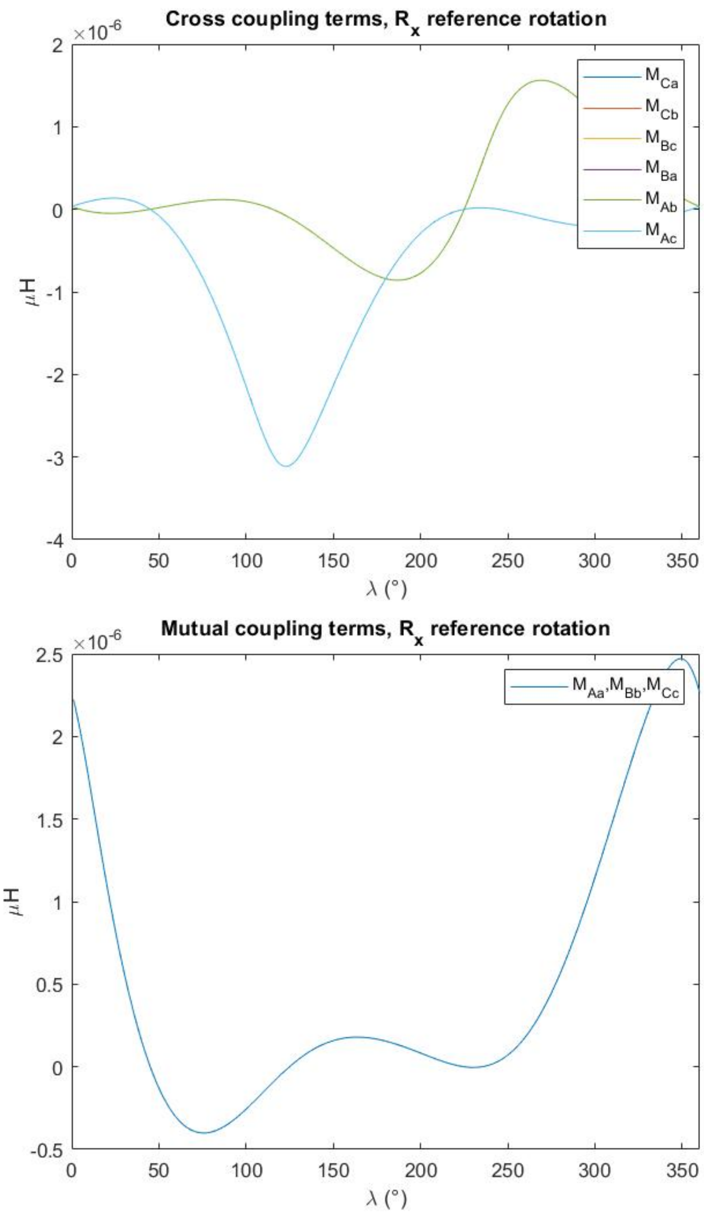

Figure 5.10. Direct and cross-coupling inductances trends for different angular positions of the receiving pad

of pad Rx around the center of gravity of Tx; in particular:

$$\begin{cases} M_{aC} = M_{bA} = M_{cB} \\ M_{aB} = M_{bC} = M_{cA} \end{cases} \tag{5.10}$$

The second plot, on the other hand, represents direct mutual inductances, which are equal to each other again due to symmetries. The case examined, however, is largely simplified due to the assumptions considered: the rotation around the origin of the fixed reference system, i.e. in $\vec{z}$, generates symmetries between the movements of the coils that I would not find in case of rotation around another generic axis.

5.4.5 x-y-λ misalignment

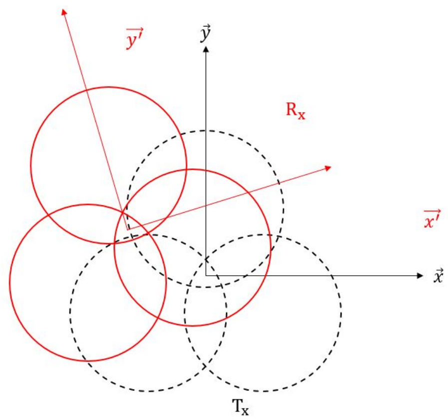

Figure 5.11. Generic x-y-λ misalignment

The addition of the possible rotation of Rx in generic cases makes the coupling matrix more complex.
Using always a Matlab code, an analysis of magnetic couplings was carried out in case of mixed misalignment, considering both rotation of Rx pad and Rx center of gravity displacement: in this regard, it was considered the position ($x = 5cm$, $y = 5cm$) for the Rx pad, and the direct inductances have been mapped as the angle of rotation varies. The results obtained are depicted in Fig.5.12.
In this case, the trends of direct inductances are not the same of the previous case; they all have different behavior, intersecting only at the points where they are null, i.e. at $\alpha_{over} = \frac{\pi}{4} + k\pi$, and at the initial position

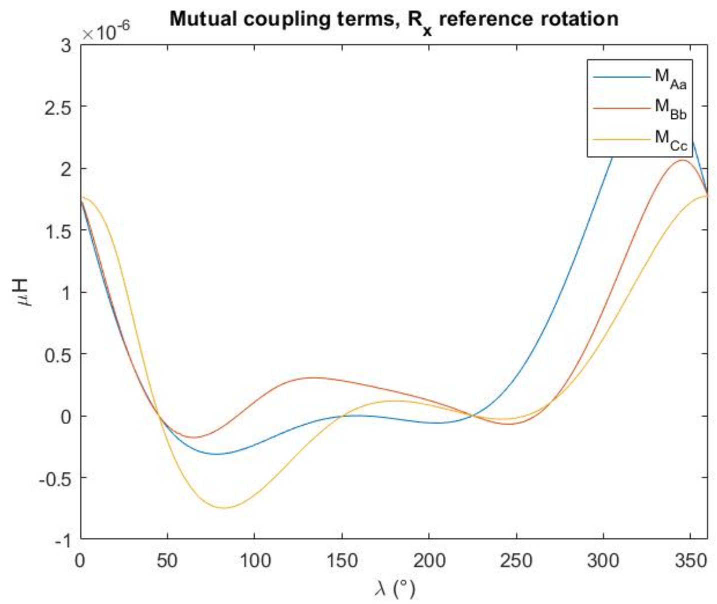

Figure 5.12. Direct inductances trends for different angular positions of the receiving pad, generic x-y misalignment case

$(\alpha_{over} = 0, 2k\pi)$.

Chapter 6

Electrical Analisys

In the various cases of misalignment analyzed, the matrix $[M]$ turns out to be more complex than in the case of perfect alignment.
In the case of generic (x, y, Λ) displacement, all the non co-planar coefficients are different. The matrix begin simplified when simmetries occur:

- In the case of $\vec{x}$-axis displacement, there are 4 different values for the 6 cross-coupling coefficients;

- In the case of $\vec{y}$-axis displacement, there are only 3 different values for the 6 cross-coupling coefficients;

- In the case of rotation of Rx around $\vec{z}$-axis, the matrix would be even more simplified, with only 2 different values between the 6 non-homologous coupling terms;

- In a generic case of x-y misalignment with rotation of Rx, the matrix becomes more complex: if in fact the rotation of Rx is combined with a displacement of its center of gravity, no symmetry is maintained, and all 6 non-homologous coefficients will be different.

The complexity of the coupling matrix translates also into complexity of the electrical system behavior; if I consider a generic system of 6 mutually coupled inductors, whose coupling matrix structure has already been identified in the previous chapters, they will be electrically representable by this matrix equation:

$$\begin{bmatrix} \hat{V}_a \\ \hat{V}_b \\ \hat{V}_c \\ \hat{V}_A \\ \hat{V}_B \\ \hat{V}_C \end{bmatrix} = j\omega_0 \cdot \begin{bmatrix} L & 0 & 0 & -M_{aA} & -M_{aB} & -M_{aC} \\ 0 & L & 0 & -M_{bA} & -M_{bB} & -M_{bC} \\ 0 & 0 & L & -M_{cA} & -M_{cB} & -M_{cC} \\ M_{Aa} & M_{Ab} & M_{Ac} & L & 0 & 0 \\ M_{Ba} & M_{Bb} & M_{Bc} & 0 & L & 0 \\ M_{Ca} & M_{Cb} & M_{Cc} & 0 & 0 & L \end{bmatrix} \cdot \begin{bmatrix} \hat{I}_a \\ \hat{I}_b \\ \hat{I}_c \\ \hat{I}_A \\ \hat{I}_B \\ \hat{I}_C \end{bmatrix} \tag{6.1}$$

The vector $[\hat{V}]$ represents the voltages applied to the ends of the individual coils, with the voltages $\hat{V}_A, \hat{V}_B$ and $\hat{V}_C$ being zero if the receiver is assumed to act only as a passive load; $[\hat{I}]$ is instead the vector of currents flowing through the coils themselves.
In the case of the optimal overlap angle α_{over}, and with the reactive compensation of the self-inductances, the coupling matrix and the system of equations undergo a simplification; thanks to this, the electrical equations of the coils are only dependent on the currents of the other pad, and the system can be described by two decoupled sub-systems of equations:

$$\begin{cases} \hat{V}_a = -j\omega_0 \cdot (M_{aA}\hat{I}_A + M_{aB}\hat{I}_B + M_{aC}\hat{I}_C) \\ \hat{V}_b = -j\omega_0 \cdot (M_{bA}\hat{I}_A + M_{bB}\hat{I}_B + M_{bC}\hat{I}_C) \\ \hat{V}_c = -j\omega_0 \cdot (M_{cA}\hat{I}_A + M_{cB}\hat{I}_B + M_{cC}\hat{I}_C) \end{cases} \tag{6.2}$$

$$\begin{cases} \hat{0} = j\omega_0 \cdot (M_{Aa}\hat{I}_a + M_{Ba}\hat{I}_b + M_{Ca}\hat{I}_c) \\ \hat{0} = j\omega_0 \cdot (M_{Ab}\hat{I}_a + M_{Bb}\hat{I}_b + M_{Cb}\hat{I}_c) \\ \hat{0} = j\omega_0 \cdot (M_{Ac}\hat{I}_a + M_{Bc}\hat{I}_b + M_{Cc}\hat{I}_c) \end{cases} \tag{6.3}$$

These equations, in the case of perfect alignment between the two tripolar systems, are further simplified:

$$\begin{cases} \hat{V}_a = -j\omega_0 \cdot (M_{aA}\hat{I}_A) \\ \hat{V}_b = -j\omega_0 \cdot (M_{bB}\hat{I}_B) \\ \hat{V}_c = -j\omega_0 \cdot (M_{cC}\hat{I}_C) \end{cases} \qquad \begin{cases} \hat{0} = j\omega_0 \cdot (M_{Aa}\hat{I}_a) \\ \hat{0} = j\omega_0 \cdot (M_{Bb}\hat{I}_b) \\ \hat{0} = j\omega_0 \cdot (M_{Cc}\hat{I}_c) \end{cases} \tag{6.4}$$

In this case, the induced voltages on the Rx-side coils will only be due to the homologous Tx-currents and the respective coupling coefficients.
In the general case, the induced voltages will depend on all three transmitter pad currents and the mutual couplings.

It is from these analytical relationships that one starts for the analytical representation of any circuit model of the system, whatever the electrical connection between the coils.
In order to be able to study the effects of misalignment in the electrical system, the idea is to utilize the results obtained from the previous magnetic analysis, thus using the magnetic couplings obtained from the algorithm in Matlab as parameters within the simulated circuit.
The final objective is to find methods with which to recognize the misalignment between the two pads that make up the system using only the electrical information that can be extracted from the system. This would make it possible both to correct the position 'online', even when charging, and above all to avoid having to use additional systems, optimizing power transfer in the simplest way possible.
The types of structures in which a three-pole WPT system can be found fall into three categories, based on the mutual connections between the coils:

- Star connection

- Delta connection

- Independent coil system

Of the three, the star connection is particularly disadvantageous: in fact, in this case, the compensation capacitors would have to withstand all the voltage applied to the windings; in addition to this, since the star center is isolated, any voltage unbalances generated by the feeding inverter would lead to non-zero star-center voltages, resulting in undesirable EMI emissions.
The independent phase structure appears to have the same problem as the star connection with regard to the sizing of the resonance capacitors: however, it will be dealt with as it is the simplest to implement and, as will be seen, the one from which it is easier to obtain the information on the system's misalignment.
Finally, the model with a delta connected topology will be analyzed, the same one used to build the reference prototype.

6.1 Independent coil system

A tripolar WPT system with independent phases requires that all the coplanar coils, although connected to the same power supply, are feeded and controlled independently. This can occur if each coil is individually connected to a single-phase power converter supplying it, with all DC-Links connected in parallel.
Such a system model was proposed by Yuan Song et al. [10], as depicted in Fig.6.1.

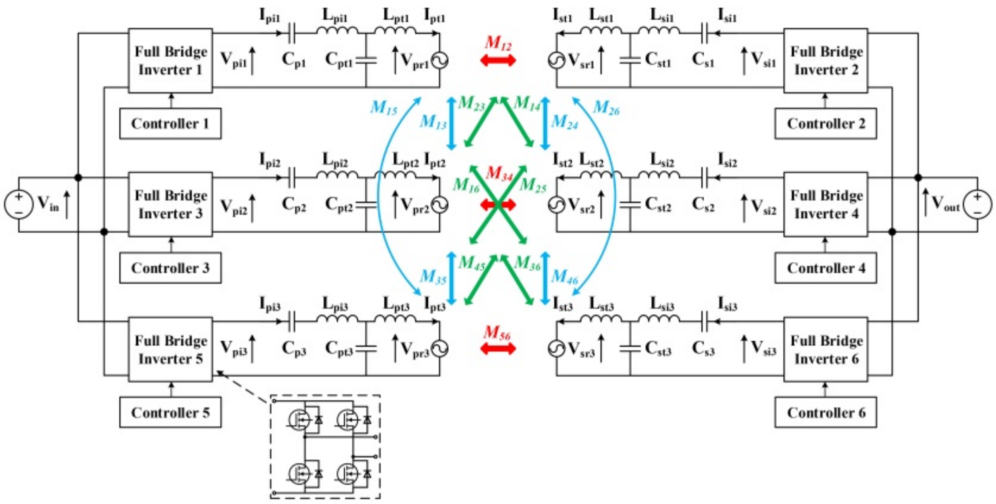

Figure 6.1. TPP-type WPT system with indipendent windings proposed by [10]

As already mentioned, this topology is the easiest to analyse: this is because the coils in the system are individually powered, and electrically disconnected from each other.
The simplified electrical equations describing the system are always those represented by 6, and in the case of resonance, the simplifications made above can be applied:

$$
\begin{cases}
\hat{V}_a = -j\omega_0 \cdot (M_{aA}\hat{I}_A + M_{aB}\hat{I}_B + M_{aC}\hat{I}_C) \\
\hat{V}_b = -j\omega_0 \cdot (M_{bA}\hat{I}_A + M_{bB}\hat{I}_B + M_{bC}\hat{I}_C) \\
\hat{V}_c = -j\omega_0 \cdot (M_{cA}\hat{I}_A + M_{cB}\hat{I}_B + M_{cC}\hat{I}_C)
\end{cases}
\tag{6.5}
$$

$$\begin{cases} \hat{0} = j\omega_0 \cdot (M_{Aa}\hat{I}_a + M_{Ba}\hat{I}_b + M_{Ca}\hat{I}_c) \\ \hat{0} = j\omega_0 \cdot (M_{Ab}\hat{I}_a + M_{Bb}\hat{I}_b + M_{Cb}\hat{I}_c) \\ \hat{0} = j\omega_0 \cdot (M_{Ac}\hat{I}_a + M_{Bc}\hat{I}_b + M_{Cc}\hat{I}_c) \end{cases} \tag{6.6}$$

The voltages applied to the coils and the currents flowing through them, used in the matrix system, are easily measurable quantities: the currents from the output of Tx-side converters and the input of Rx-side ones, and the same for the voltages applied to the coils.

6.1.1 Regular three-phase power supply

The first tests performed are those with a regular three-phase system power supply. The simplified circuit model used is shown in Fig.6.2 and was realized using the circuital simulation software PLECS, by Plexim.

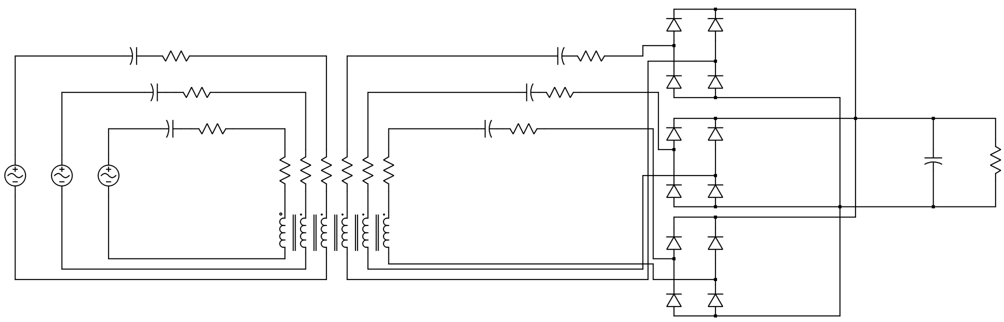

Figure 6.2. Circuit diagram of the WPT system with independent phases

The circuit provides separate power supplies for the transmitter phases, with the six inductors coupled and compensated on each side perfectly.
Downstream of the receiver coils and compensation capacitors there are three diode non-controlled rectifiers, connected in parallel to the same resistive load. To reduce the output current ripple, a simple C-filter has been adopted.
Tab.6.1 shows the main data of the simulated system.
Since the system appears to be geometrically symmetrical, it was decided to start with this important information. Both pads, as known, are constructed by overlapping three circular coils, each one equidistant from the

V_{in}	48	V
f	80	kHz
L	6.728	μH
C_{res}	588	μF
R_{cap}	2	$m\Omega$
R_{ind}	20	$m\Omega$
C_{filt}	300	μF
R_{load}	200	$m\Omega$

Table 6.1. Main parameters of the indipendent phases system simulation

center of gravity of the structure and from each other, by an angle of 120°. Thanks to this structure, we can distinguish three symmetry axes for the pad, each one passing through the origin (center of gravity of the pad) and through the center of one of the coils.
In the previous analysis concerning the magnetic interactions between coils, it was verified how a displacement along $\vec{y}$ axis would generate a simplification in the coupling matrix, with only three different values for the 6 cross-coupling terms, and this happens because symmetry plays a fundamental role on the misalignment effect. The same thing would happen, for the same reasons, if I move the receiving pad along the other two symmetry axes of the system.
The tests with regular three-phase power supply were first carried out along these symmetry axes; Fig.6.3 shows the measures of phase currents form the receiver, for 6 different misalignment positions along the symmetry axes of the system. The 6 positions chosen for the simulations share the same distance from the center of the Tx reference frame, set at $m = 10cm$. In the cases considered, there is no rotation of the receiving pad with respect to the reference axes, hence $\lambda = 0$.

Of the six graphs in the figure, the 2 at the top represents the case of misalignment along $\vec{y}$; in the middle the case of displacement along the symmetry axis passing through coil b, while at the bottom the misalignment on the symmetry axis trough coil c; the left ones and the right ones, respectively, are measures in points with $y > 0$ and $y < 0$.
From the graphs, it can be seen how, for displacements along the symmetry axis passing through a certain coil of the transmitter system, the current for that winding varies independently, while the other two always have the

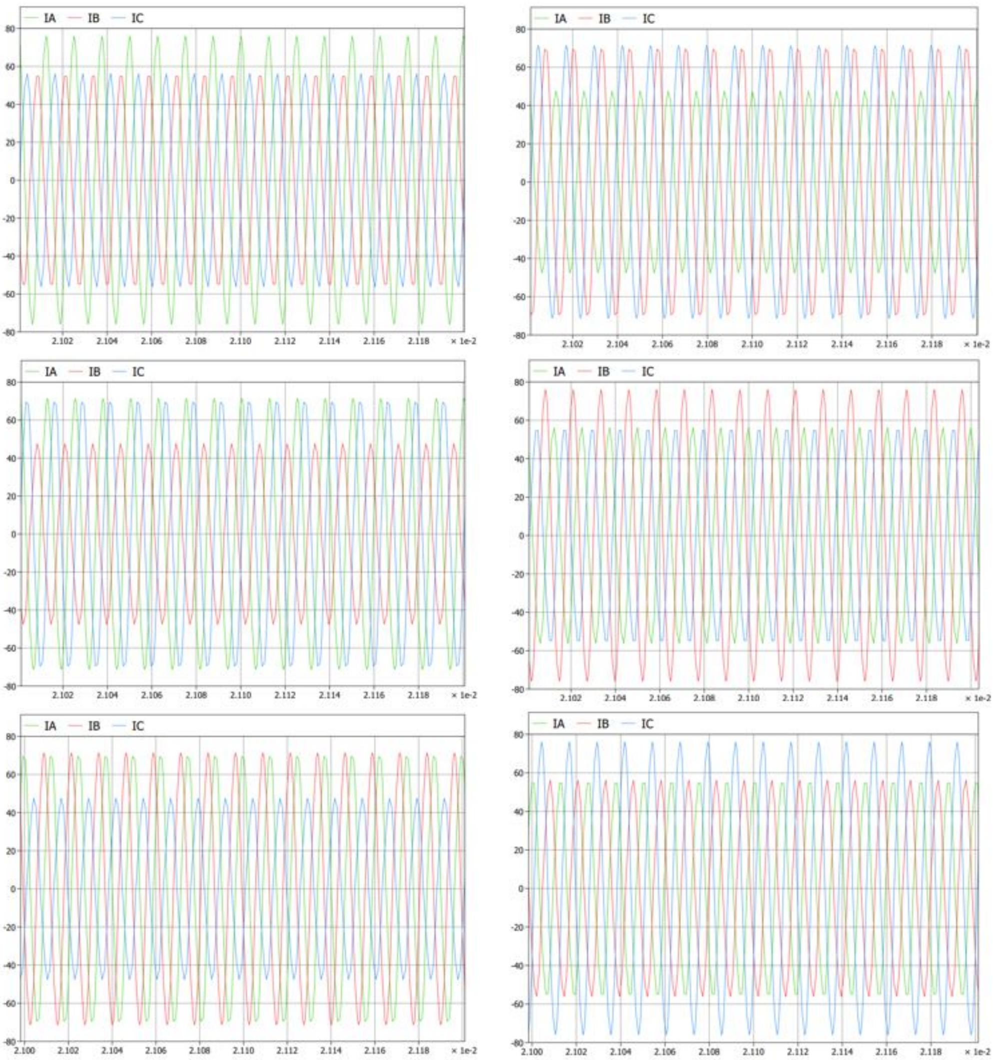

Figure 6.3. Phase currents for misalignments along the Tx pad symmetry axes

same modulus.
From further tests carried out for generic misalignments, it was possible to deduce that the receiver-side currents are strongly influenced by the behavior of the system along these axes: in particular, it is possible to subdivide the displacement field of the receiving pad into three areas of influence, each having one of the three symmetry axes of the pad as its bisector, and

each area, in turn, can be subdivided into two sub-areas delimited by the axes themselves. It was therefore possible to construct an empirical map of the displacements of the receiving pad, shown in Fig.6.4, which allows the position of the Rx pad to be recognized.

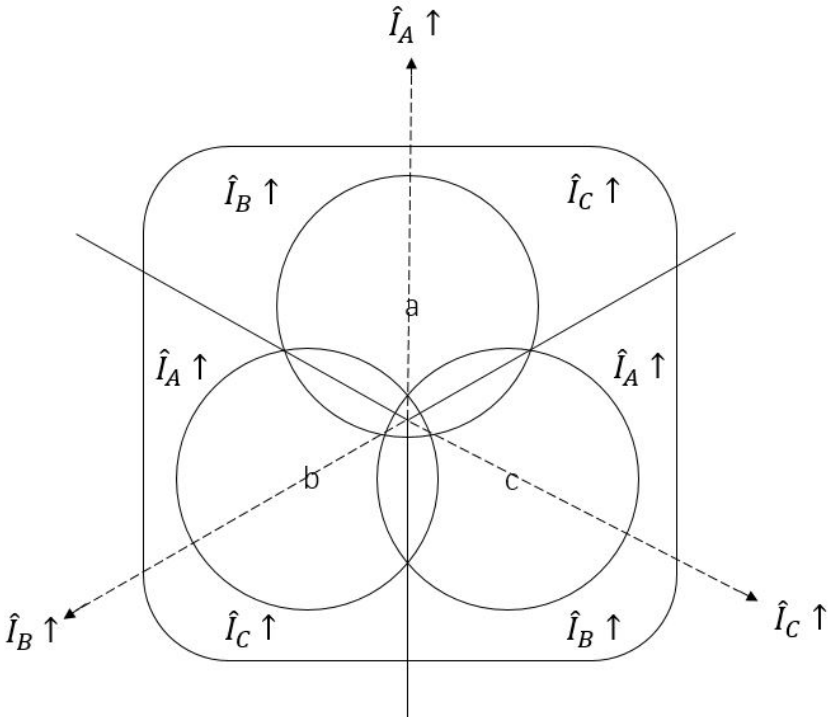

Figure 6.4.

Assuming a generic misalignment of the Rx pad with respect to the Tx reference, excluding the possibility of rotation, the map can be used in this way:

- By measuring the output currents from the receiving pad, the one with the highest modulus indicates in which of the three possible macro-zones of displacement the Rx pad is: each encompasses an angular amplitude of $\frac{2}{3} \cdot \pi$, and has as its bisector one of the axes of symmetry of the geometric structure, on the side with the positive direction, in Fig.6.4 indicated with a dotted line.

- Finally, the second current with a higher modulus defines the exact sextant in which the shift of Rx occurred, from among the two possible for each macro area.

The main advantage of this system is that it is unambiguous: knowing the three currents and their respective modules, althought it is not possible to recognise the exact position in coordinates, we can identify the area in which the pad Rx has positioned, by simply comparing the modules of the currents.

6.1.2 Single-coil supply

In order to recognize the precise position of the Rx pad, the technique devised is to feed the phases of the Tx pad individually, and alternately: in this way I can individually analyze the effects of the magnetic coupling of the fed phase with the three receiving coils.
To do this, a simplified circuit model of the system was prepared in PLECS environment (Fig.6.5). Compared to the previously used model, for simplification the three rectifiers downstream of the Rx pad have been replaced by simple phase resistors, the same for all three phases.
The six decoupled circuits of the system are individually compensated, considering the self-inductance found during numerical simulations in Matlab ($L = 6.728\mu H$) and the switching frequency set at $80kHz$. Switches have been provided in the Tx-side circuit, so that the phases are fed one at a time. Simple discharge circuits are provided for the transmitter-side inductors, to allow them to discharge once disconnected from the main circuit; downstream of the Rx inductor system, simple resistive loads are provided.

The system, consisting of six electrically decoupled circuits, can be described by the matrix of electrical equations shown above; the complete system of equations must also take into account the contribution of the resistance of the individual phases, the sum of the winding resistances, the parasitic resistances of the capacitors and the load:

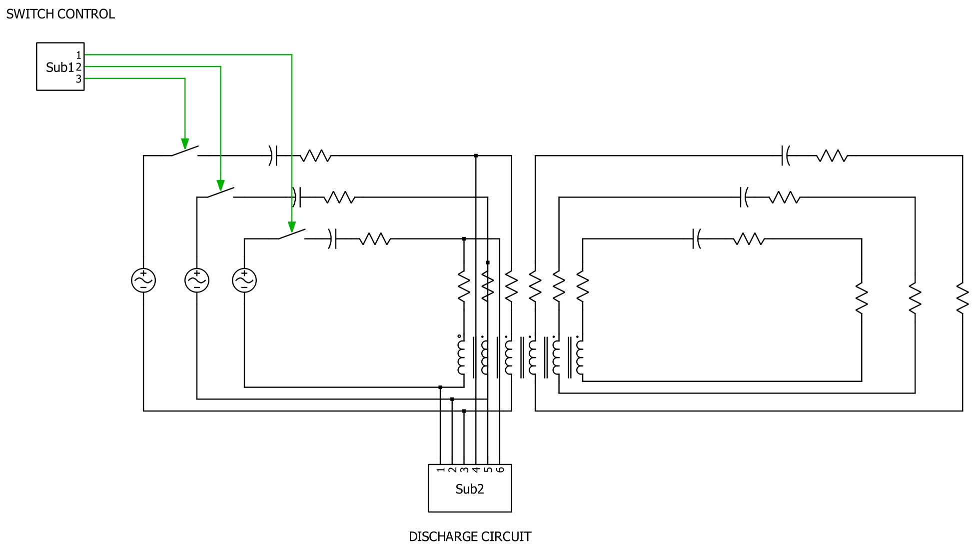

Figure 6.5. Simplified Plecs model of WPT TPP system with independent phases for alternating power supply

$$\begin{bmatrix} \hat{V}_a \\ \hat{V}_b \\ \hat{V}_c \\ \hat{0} \\ \hat{0} \\ \hat{0} \end{bmatrix} = j\omega_0 \cdot \begin{bmatrix} 0 & 0 & 0 & -M_{aA} & -M_{aB} & -M_{aC} \\ 0 & 0 & 0 & -M_{bA} & -M_{bB} & -M_{bC} \\ 0 & 0 & 0 & -M_{cA} & -M_{cB} & -M_{cC} \\ M_{Aa} & M_{Ab} & M_{Ac} & 0 & 0 & 0 \\ M_{Ba} & M_{Bb} & M_{Bc} & 0 & 0 & 0 \\ M_{Ca} & M_{Cb} & M_{Cc} & 0 & 0 & 0 \end{bmatrix} \cdot \begin{bmatrix} \hat{I}_a \\ \hat{I}_b \\ \hat{I}_c \\ \hat{I}_A \\ \hat{I}_B \\ \hat{I}_C \end{bmatrix} + R_{ph} \cdot \begin{bmatrix} \hat{I}_a \\ \hat{I}_b \\ \hat{I}_c \\ \hat{I}_A \\ \hat{I}_B \\ \hat{I}_C \end{bmatrix} \tag{6.7}$$

$$R_{ph} = R_{cond} + R_{coil} + R_{load} \tag{6.8}$$

The switch control on Tx-side is designed to have three separate feeding steps:

- Step 1: Only coil a on the Tx side is powered, with the Rx-side windings all connected to the main circuit. By doing this I will derive the modulus of M_{Aa}, M_{Ba}, M_{Ca} from the system:

$$|M_{Aa}| = \frac{R_{ph}}{\omega_0} \cdot \frac{|\hat{I}_A|}{|\hat{I}_a|} \qquad |M_{Ba}| = \frac{R_{ph}}{\omega_0} \cdot \frac{|\hat{I}_B|}{|\hat{I}_a|} \qquad |M_{Ca}| = \frac{R_{ph}}{\omega_0} \cdot \frac{|\hat{I}_C|}{|\hat{I}_a|} \tag{6.9}$$

- Step 2: Only coil b on the Tx side is powered, with the Rx-side windings all connected to the main circuit. By doing this I will derive the modulus of M_{Ab}, M_{Bb}, M_{Cb} from the system:

$$|M_{Ab}| = \frac{R_{ph}}{\omega_0} \cdot \frac{|\hat{I}_A|}{|\hat{I}_b|} \qquad |M_{Bb}| = \frac{R_{ph}}{\omega_0} \cdot \frac{|\hat{I}_B|}{|\hat{I}_b|} \qquad |M_{Cb}| = \frac{R_{ph}}{\omega_0} \cdot \frac{|\hat{I}_C|}{|\hat{I}_b|} \tag{6.10}$$

- Step 3: Only coil c on the Tx side is powered, with the Rx-side windings all connected to the main circuit. By doing this I will derive the modulus of M_{Ac}, M_{Bc}, M_{Cc} from the system:

$$|M_{Ac}| = \frac{R_{ph}}{\omega_0} \cdot \frac{|\hat{I}_A|}{|\hat{I}_c|} \qquad |M_{Bc}| = \frac{R_{ph}}{\omega_0} \cdot \frac{|\hat{I}_B|}{|\hat{I}_c|} \qquad |M_{Cc}| = \frac{R_{ph}}{\omega_0} \cdot \frac{|\hat{I}_C|}{|\hat{I}_c|} \tag{6.11}$$

In the case where there is no rotation of the receiving pad, the number of calculations to be performed can be reduced by calculating only one of the homologous mutual inductance coefficients, as the other two will be identical, for the reasons explained previously.
These analytical results are confirmed by the circuit simulations performed. Fig.6.6 shows the trends of the currents on the Tx side (top) and Rx side (bottom), with the steady-state operation of the charging system at the end of the simulation.

Having found the moduli of the coupling coefficients, however, the signs are still unknown. This means that it is not yet possible to determine the exact position of the receiving pad, as the inductance matrix is not known unambiguously.
Here again, we can make analytical considerations, generalising the formulas just used to calculate $[M]$, returning to phasor notation:

$$M_{RT} = -\frac{R_{ph}}{\omega_0} \cdot \frac{\hat{I}_R}{\hat{I}_T} \tag{6.12}$$

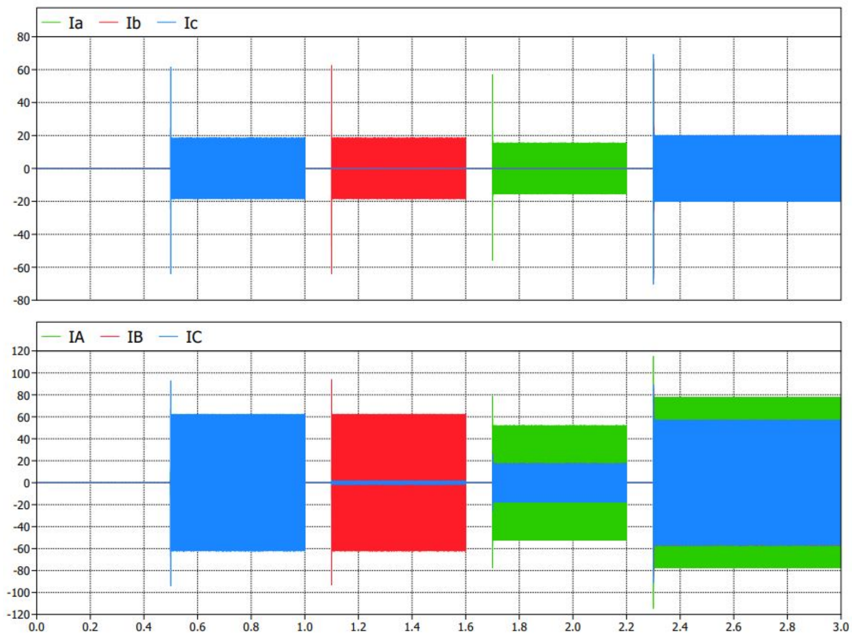

Figure 6.6. Tx coils currents (top) and Rx (bottom) during 3-step test

Where subscript T identifies a coil of Tx, R an Rx one. Assuming that the area of possible mismatch is limited, I can assume that the mutual homologous inductances do not change significantly but always remain positive. This means that, since the three receiver-side circuits are resistive-inductive loads, the phasors of the currents on the Rx-side will lag behind the $\vec{V}$ phasor of the voltage induced on the single coil, by a generic angle φ (Fig.6.7).
Since the system is perfectly compensated on both sides, the three induced voltages on the Rx side differ only in the modulus but will have the same phase. Consequently, I will have that:

- If the non-homologous phase currents are in phase with the homologous phase current, then their respective mutual inductances are positive;
- If the non-homologous phase currents are in phase opposition to the homologous one, then their coupling coefficients are negative.

An idea to implement it could be to measure the modules of currents

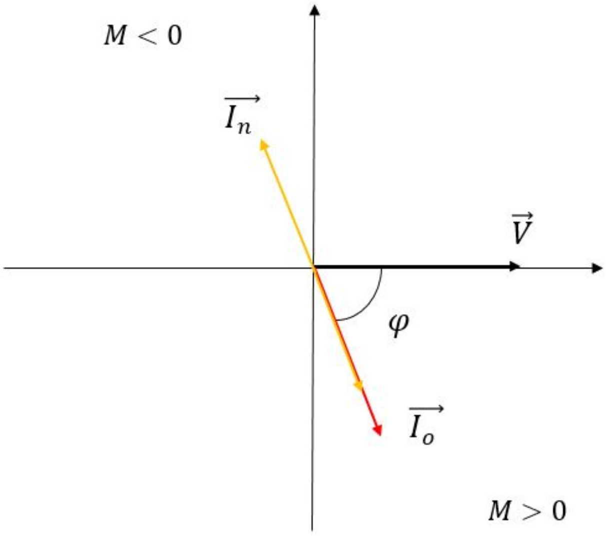

Figure 6.7. Phasor representation of homologous ($\vec{I_o}$, in red) and non-homologous ($\vec{I_n}$, in yellow) Rx-side currents in case of positive or negative mutual coupling.

and at the same time also detect the presence of their peaks, verifying whether the maximum and minimum values of the compared signals occur at different times or at the same time; in any case, the implementation of such a system is not taken into account for this thesis work, and could be investigated in future works.
As an example, Fig.6.8 shows the current waveforms of the system in the test case with pad Rx positioned at $y = 10cm$: at the bottom the waveforms of the output currents on the Rx side, at the top that of the current of the only active phase, $\vec{I_b}$. The receiving phase with the largest current is the homologous one, while the other two are the non-homologous ones, and both are in phase opposition respect to the first, due to the negative sign of the coupling coefficients ($M_{Bb} = 1.49\mu H$, $M_{Ab} = -216nH$, $M_{Cb} = -38nH$).

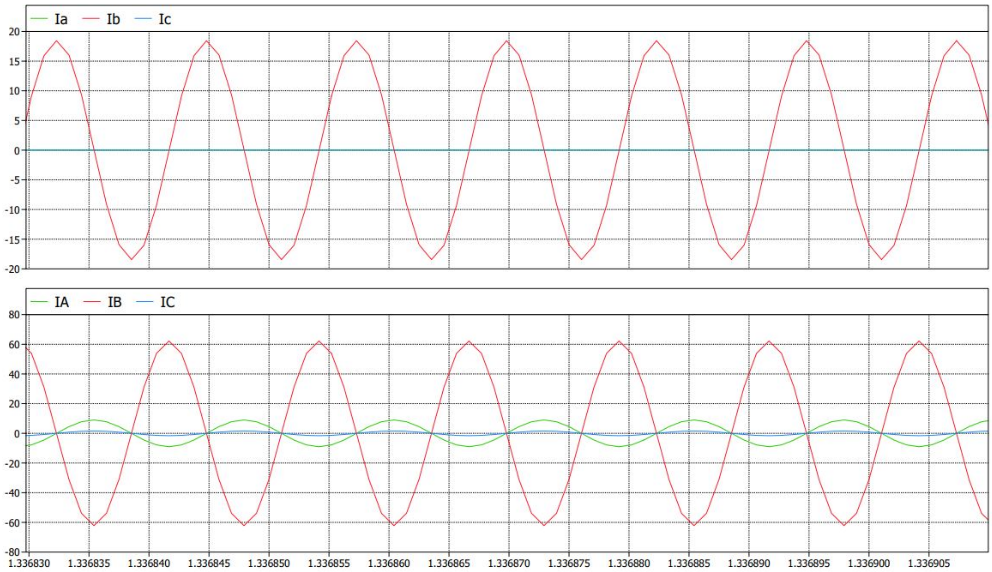

Figure 6.8. Detail of the Tx current of the active phase (coil b) and the induced currents on the Rx side.

6.1.3 Practical issues

The system configuration just used, although it is optimal for mismatch detection, appears to have limitations from a practical point of view: firstly, such a solution requires the use of no less than three transmitter-side active power converters, most likely Full Bridge Inverters, to enable the three phases to be supplied separately, when it would be possible to supply the system with a single three-phase Full Bridge Inverter. This implies higher costs, but also presumably lower efficiency, as 12 power switches would be used instead of 6 in the case of a three-phase power inverter.
Furthermore, the filter capacitors will be subjected to the same voltage of the coils, which makes them bulky and difficult to be sourced.

6.2 Delta connected topology

The second circuit configuration considered in our study is the one used for the reference WPT TPP prototype, developed in the PEIC laboratories at the Politecnico di Torino. The circuit model proposed in Fig.6.9 reproduces

its main characteristics in detail.
It is powered by a DC voltage source to which the DC-link of the three-phase inverter is connected and which powers the transmitter pad.

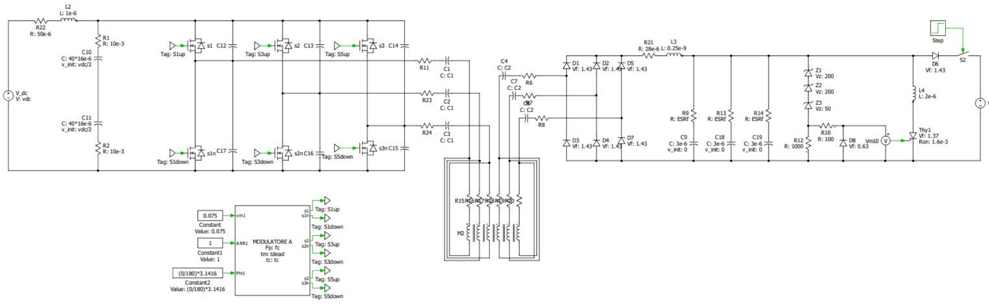

Figure 6.9. WPT circuit diagram with delta coil connection [4]

The inverter has the task of generating the three line voltages at the input to the transmitter pad, using a six-step control with phase-shifted modulators, so that the three line voltages are perfectly balanced and phased by 120°.

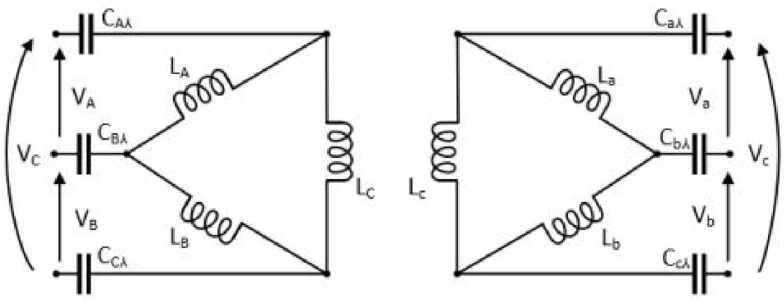

Figure 6.10. $YC - \Delta L$ circuit diagram

The compensation capacitors for the resonance are connected in a star configuration, outside the coil triangle (Fig.6.11): in this way, they will be subjected to approximately 70% less stress in terms of peak voltage, compared to a connection in series to the windings and inside the triangle [3]. For this reason, we can define the system as $YC - \Delta L$ [2]. The only negative note of this connection is the necessary compensation capacity, which is increased, as for Eq. 6.13 [4]:

$$C_{ph,ext} = 3C_{ph} = \frac{3}{\omega_0^2 \cdot L_{ph}} \tag{6.13}$$

where ω_0 is the switching frequency chosen for the system, which is $80kHz$, while the term L_{ph} is the self-inductance of each individual coil.
The mutually coupled coil system was represented with 6 mutually coupled inductors, with the coupling coefficients represented by the well-known matrix $[M]_{6x6}$.
At the output of the Rx pad, an undriven diode rectifier, a filter stage for the rectified current, and finally a DC voltage generator as a simplified battery model are cascaded.

6.2.1 System simulation

As mentioned before, this system topology has many advantages from a practical and implementation point of view, especially compared to the one previously considered.
At the same time, however, this configuration is more disadvantageous for the detection of misalignment: it is not possible in this case to power one coil at a time of the transmitter and thus driving the windings individually.

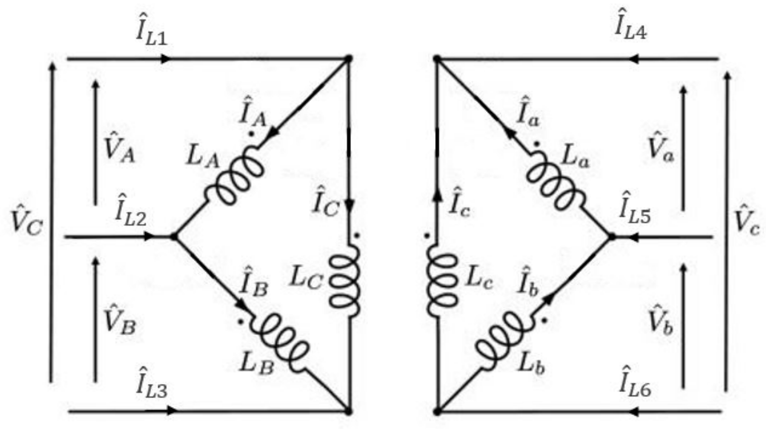

Figure 6.11. Equivalent circuit model with line and phase currents

Fig.6.11 shows the connection diagram between coils and resonance capacitors on the Tx and Rx side in the system under consideration. The system again can be described with the matrix equation 6, but the currents vector $[\hat{I}]$ indicates the currents flowing through the individual coils, i.e. those within the triangle in both pads; the voltages applied to each coil are precisely the line voltages applied by the three-phase inverter to the transmitting system.
Since it is a three-phase system, the relationships linking the line currents to those of the individual coils result:

$$\begin{cases} \hat{I}_{L1} = \hat{I}_a + \hat{I}_c \\ \hat{I}_{L2} = \hat{I}_b - \hat{I}_a \\ \hat{I}_{L3} = -\hat{I}_b - \hat{I}_c \end{cases} \qquad \begin{cases} \hat{I}_{L4} = \hat{I}_A + \hat{I}_C \\ \hat{I}_{L5} = \hat{I}_B - \hat{I}_A \\ \hat{I}_{L6} = -\hat{I}_B - \hat{I}_C \end{cases} \tag{6.14}$$

Furthermore, since it is a balanced three-phase system, the line currents will have zero-sum at each instant of time, thus:

$$\begin{cases} \hat{I}_{L1} + \hat{I}_{L2} + \hat{I}_{L3} = 0 \\ \hat{I}_{L4} + \hat{I}_{L5} + \hat{I}_{L6} = 0 \end{cases} \tag{6.15}$$

The main problem with the delta connection can be deduced from the relations just written: coil currents cannot be derived from line currents, whereas it is possible to do the opposite; in practice, however, the only currents that can be measured are those outside the pads.
The consequence of these two problems is that it will not be possible to solve the system of electrical equations analytically as in the previous case. In order to analyze the effects of misalignment on the system's electrical quantities, it was therefore decided to start with the analysis in the case of a regular three-phase supply, and then to study an alternative supply case, referred to as 'opposing voltages'.

6.2.2 Regular three-phase power supply

As is already known, it is not possible to analytically derive from the magnetic equations the values of the mutual inductances at a generic position of the receiving pad with respect to the transmitter.
However, it is well known that the system under study has three symmetry axes, and displacements along these straight lines can provide useful information on electrical quantities. It was therefore decided to analyze the

trends of Tx and Rx line currents for displacements along these characteristics.

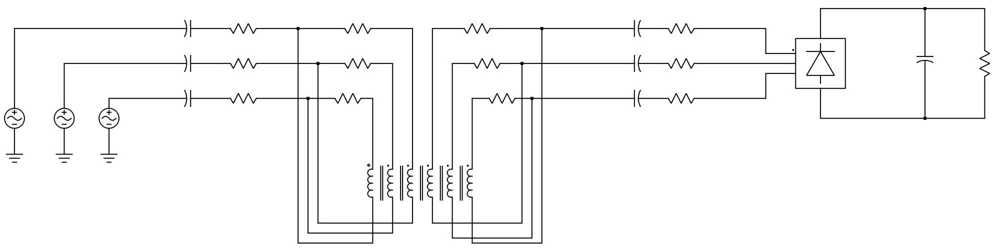

Figure 6.12. Simulated circuit, regular three-phase power supply

The system used in the simulation is depicted in Fig.6.14: the transmitting pad, represented by three of the six mutually coupled inductors, is powered by three separate single-phase generators which impose the set voltage on each magnetic winding.
As in the real system, the compensation capacitors have been placed in a $YC - \Delta L$ configuration, although it is not influent for the simulation purpose; on the Rx side, the system is connected to an uncontrolled three-phase rectifier, with a purely resistive load downstream, preceded by a filtering capacitor, in order to minimize the current ripple on the load. Tab.6.2 shows the main values used for the simulation.

V_{in}	20	V
f	80	kHz
L	6.728	μH
C_{res}	$3 \cdot 588$	μF
R_{cap}	2	$m\Omega$
R_{ind}	20	$m\Omega$
C_{filt}	300	μF
R_{load}	200	$m\Omega$

Table 6.2. Main parameters, delta connected system

In particular, the first six tests were all performed at a distance $m = 10cm$ from the center of gravity of Tx, each at the six corresponding points of the three lines of symmetry. Fig.6.14 shows the trends of the Rx-side line currents for the chosen misalignment points: at the top the points along the symmetry axis for coil b, in the middle those along the axis for c, at the bottom those along $\vec{y}$. The graphs on the right are for the misalignment points with positive ordinate, and those on the left are those with a negative coordinate.

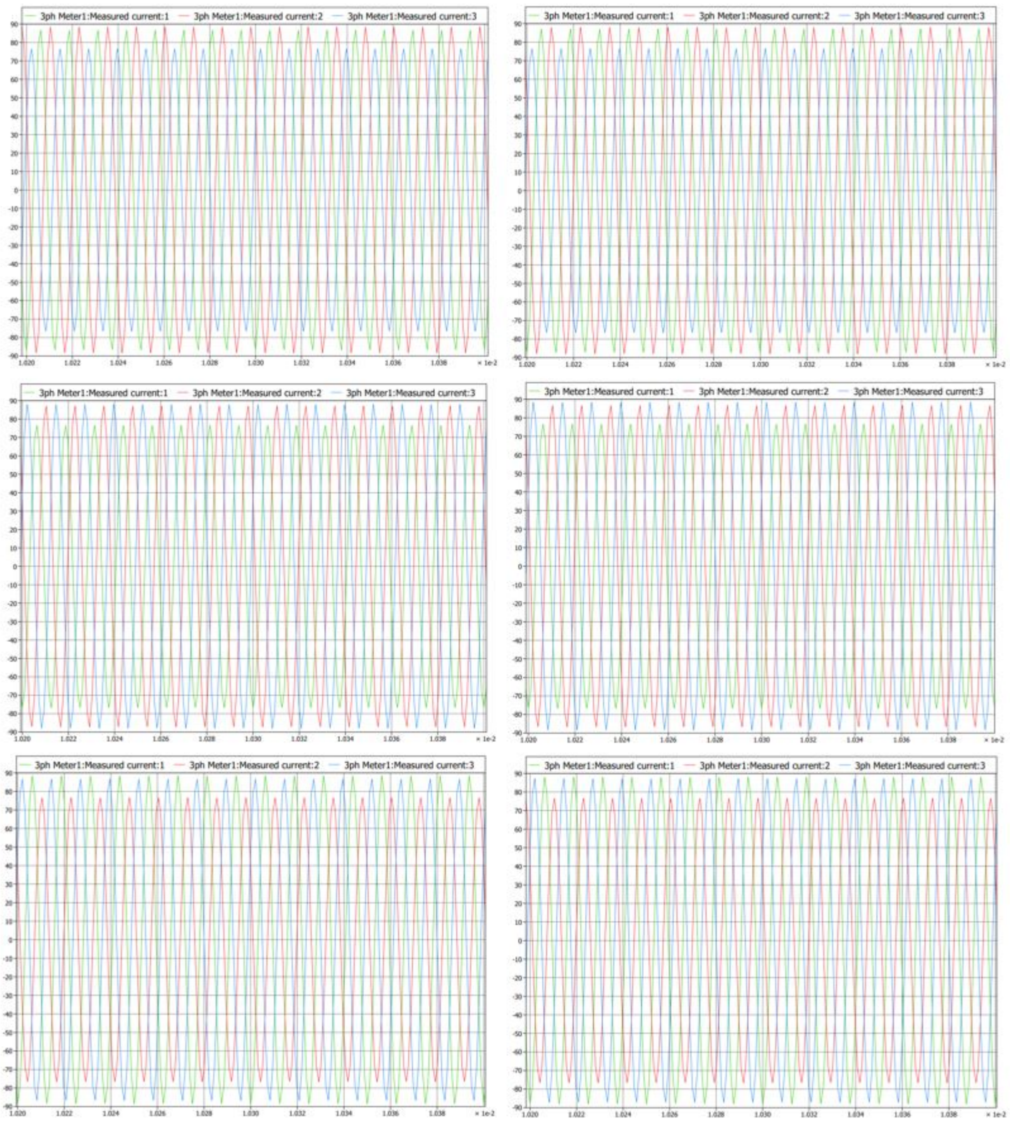

Figure 6.13. Rx-side line currents for misalignments along symmetry axes, regular three-phase supply

What is noticeable is that for points belonging to the same axis of symmetry and in mirrored position, the course of the currents is identical; this means that, in the case of misalignment of the receiving pad along these axes, it is not possible to recognize the position unambiguously by knowing only the currents outgoing from the receiving pad, with the three-phase regular supply. It is possible to determine the specific axis in which the pad's displacement occurred; however, this type of information is not decisive from a practical point of view, since typical misalignment in a WPT system occurs at generic positions in the $\vec{x} - \vec{y}$ plane, so it is necessary to investigate the effects of misalignment at generic positions.
In this regard, several simulations have been carried out considering the positioning of the center of gravity of Rx at generic points on the plane, under the simplifying hypothesis of non-rotation of the receiver system; by collecting the related data, an interesting behaviour of the system could be outlined: also in this case, as for the system with independent phases, the currents at the output of the receiver, in case of misalignment, are influenced by the behavior in the closest symmetry axes.
In particular, the closer the pad's stationary point is to one of the two delimiting symmetry axes, the closer the modules of the three output currents will be to those experienced on the axis, on the point at equal distance from the origin of the reference system.
In this case too, it was possible to represent a map (Fig.6.14), similar to the one used previously for the system with independent phases, but with different usage criteria.
The map in question can be used in the following way:

- The lowest measurable output current on the Rx side is the same that can be experienced moving along the closest symmetry axis; the proximity to one of the two axes delimiting the six areas is considered in angular terms;

- The second lowest output current is the lowest that can be experienced moving along the other symmetry axes delimiting the area.

By doing so, it is possible to divide the displacement area of Rx into 12 sub-areas, 2 for each *"sextant"* delimited by the axes.
This behavior was also verified for the currents entering the transmitter pad, which were included in the map represented.

However, some problems remain open with this strategy:

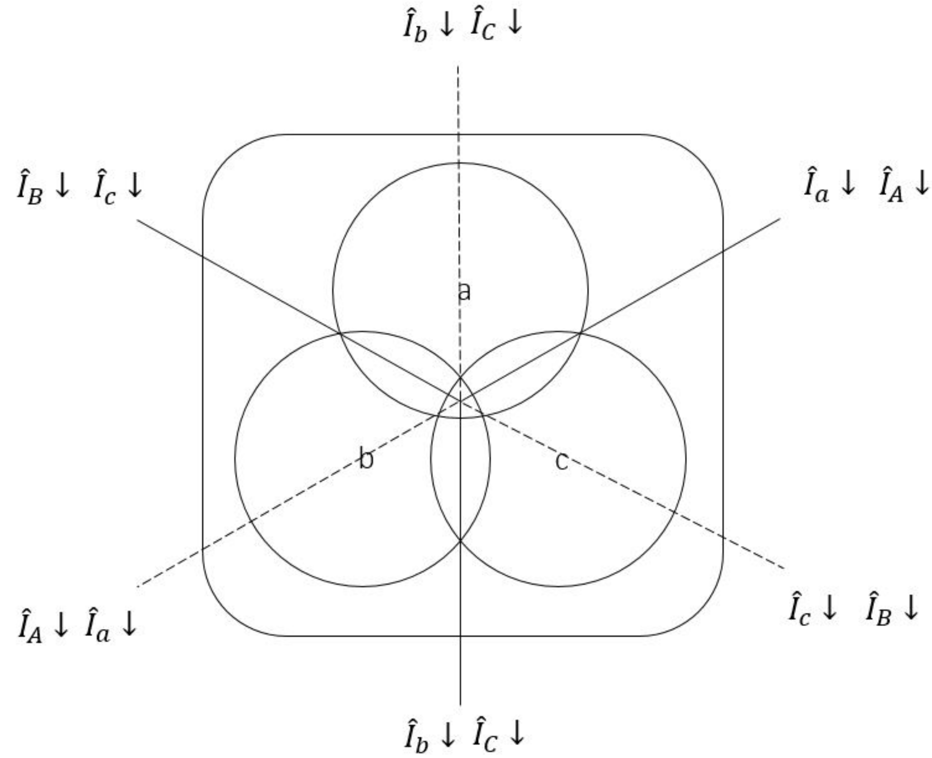

Figure 6.14. Displacement map with Tx-Rx line currents, regular three-phase power supply

- Possibility to recognise the precise positioning point

- Eliminating ambiguity between equivalent points

Setting aside the first problem, which is left to possible future investigations, the second stems from the fact that, knowing any set of three line Tx and Rx currents, there is no univocal area of possible displacement, but two possible areas mirroring each other with respect to the origin of the system's reference axes. The correct stationing area of the receiving pad, therefore, cannot be determined by the line currents of the system only.

6.2.3 Opposing voltages supply

The main constraint to be observed when supplying a three-phase delta load, as is well known, is that the sum of the line voltages at each instant of time must be zero: this is because the KVL (Kirchhoff Voltage Law) must be valid in the closed circuit bounded by the triangle of the three interconnected coils.
The system can therefore only be powered by voltages whose phasors have zero-sum. With the regular three-phase supply this is verified, but its limitations in recognizing the relative mismatch between the pads are well known. An alternative method can then be to supply the system with 'opposing voltages'.

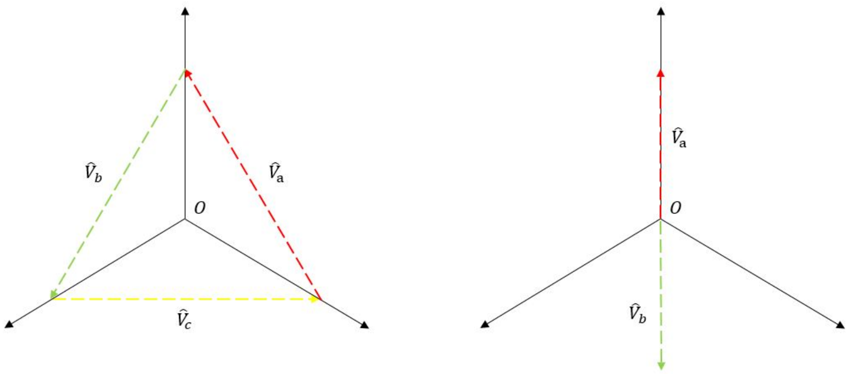

Figure 6.15. Line voltages phasor representation: regular three-phase supply (left) and opposing voltages supply (right)

The phasor diagram of this kind of power supply is depicted in Fig.6.15. It requires that two of the concatenated input voltages are imposed with the same modulus but in phase opposition: thus the two voltages have a zero sum, and the third voltage is zero in turn.
The simulation schematic is shown in Fig.6.16 and is identical to that used for the three-phase power supply, with the only difference being the voltage generators used at the input; in the previous case, three voltage generators were used with a phase offset of $\frac{2}{3}\pi$; in this case, two input generators with voltages of the same module and the same phase are used to reproduce the proposed phasor scheme. The moduli of the voltages also remain unchanged from the previous case.

Of the three possible combinations, we choose in simulation to make $\vec{V}_c$

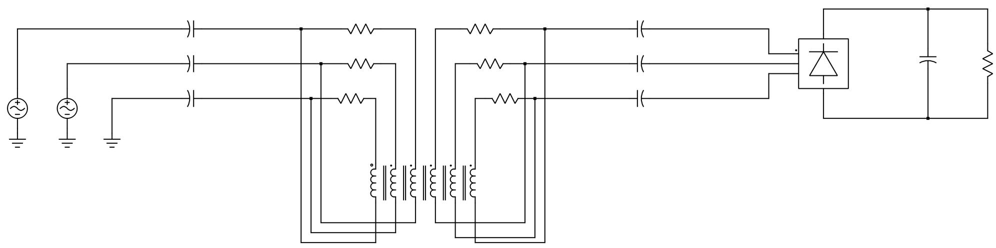

Figure 6.16. Simulation diagram, power supply with opposing voltages

null. In the case of perfect alignment between the two pads, imposing null supply voltage to the coil means that no current will flow in it, and the same thing happens to its homologous counterpart on the receiving pad. This phenomenon can be explained by the electrical equations for the two coils considered:

$$\begin{aligned} \hat{V}_c &= -j\omega_0 \cdot (M_{cA}\hat{I}_A + M_{cB}\hat{I}_B + M_{cC}\hat{I}_C) \\ \hat{V}_C &= j\omega_0 \cdot (M_{Ca}\hat{I}_a + M_{Cb}\hat{I}_b + M_{Cc}\hat{I}_c) \end{aligned} \tag{6.16}$$

$\hat{V}_c$ and $\hat{V}_C$ are both null, one because of the power supply hypothesis made, the other because it is connected to a purely passive load; moreover, all the cross-coupling coefficients are null in perfect alignment, so the currents flowing through those branches are negligible; as a direct consequence, among the line currents measurable both on the Tx and Rx side, two of them will be identical in magnitude and phase, while the other will be of the same magnitude but in phase opposition, as visible in Fig.6.17.

In the case of misalignment, the system behavior will be different: the supply voltages applied to the two branches will always be null, but the mutual coupling coefficients will be non-null. In the Rx-side coil, this will cause an induced voltage, and a non-zero current will consequently flow through it. In turn, the homologous coil on the Tx side will also be affected by variable fluxes, which generate an induced voltage and current.

It can be interesting to analyze the trend of the current flowing into the non-fed coil, in order to find the degree of misalignment of the system: for this reason, it was decided to carry out simulations on the equivalent circuit with this alternative supply. The analysis was carried out for displacements along the axes of symmetry in the first instance, and then other generic displacements were considered.

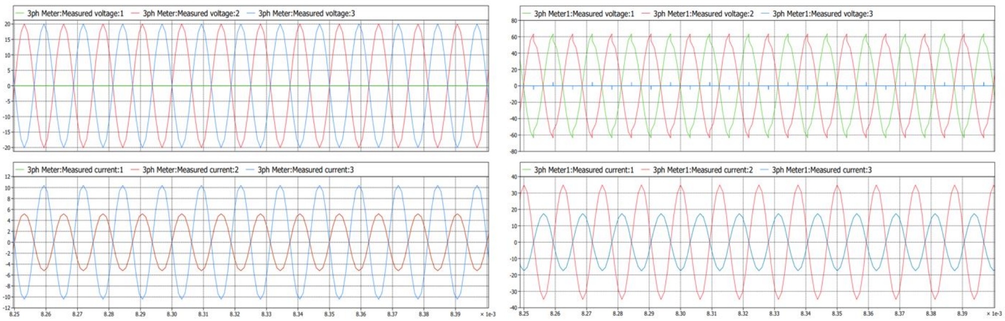

Figure 6.17. Line currents and voltages on Tx (left) and Rx (right) side of WPT system with delta connection

Misalignment along symmetry axes

The first tests performed are those along the symmetry axes of the system. To perform the simulations along the axes, the circuit of Fig.6.16 was used, with $\hat{V}_a = -\hat{V}_b$ and $\hat{V}_c$ null respectively.
The graphs in Fig.6.19 show the line currents on the transmitter and receiver side; note that only 2 of the 3 have been graphed, as the third is the sum of them. In Fig.6.18, on the other hand, the currents of the non-fed coils have been graphed.

As far as the line currents are concerned, it can be seen from the graphs in Fig.6.19 that with respect to the position of perfect alignment, the negative and positive ordinate trends are perfectly mirror-imaged: this means that as with the regular three-phase power supply, it is not possible to distinguish between two mirror-image positioning points belonging to the same axis.
For displacements along the symmetry axis passing through coil b, analyzing the results it is possible to notice a system behavior quite similar to the one in perfect alignment condition: the current of the two non-fed coils is zero, while the two measured line currents have the same modulus. This condition can be explained by the electrical equation for the excluded coil on the Rx side:

$$\hat{0} = j\omega_0 \cdot (M_{Ca}\hat{I}_a + M_{Cb}\hat{I}_b) \rightarrow M_{Ca}\hat{I}_a = -M_{Cb}\hat{I}_b \tag{6.17}$$

The currents flowing in the other two coils are in phase opposition and

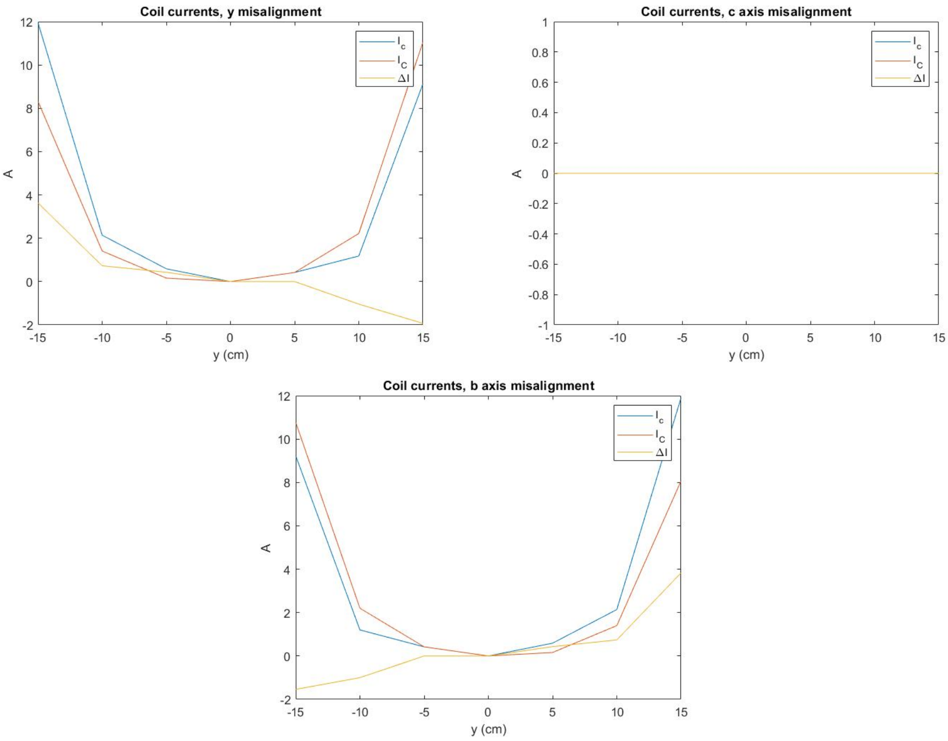

Figure 6.18. $\hat{I}_c$ and $\hat{I}_C$ trends for misalignments along the three symmetry axes

with the same modulus, while the coupling coefficients M_{Ca} and M_{Cb} are equal because the displacement occurs along the symmetry axis passing through coil b.
In general, by choosing one of the three possible feeds with opposing voltages, there will always be one of the axes of symmetry that will allow this result, with two homologous coil currents being null. In Fig.6.20, a simplified representation of the effects of changing the non-fed coil has been shown: the axis along which a null current is measured corresponds to the one passing through the excluded coil.
The tests of misalignment along $\vec{y}$ show instead that it is possible to discriminate between points of misalignment with positive ordinate and those with a negative one: in the first case, the magnitude difference ΔI between the current on Tx-side coil and the one on Rx-side, is negative; in the second case instead the ΔI is positive.

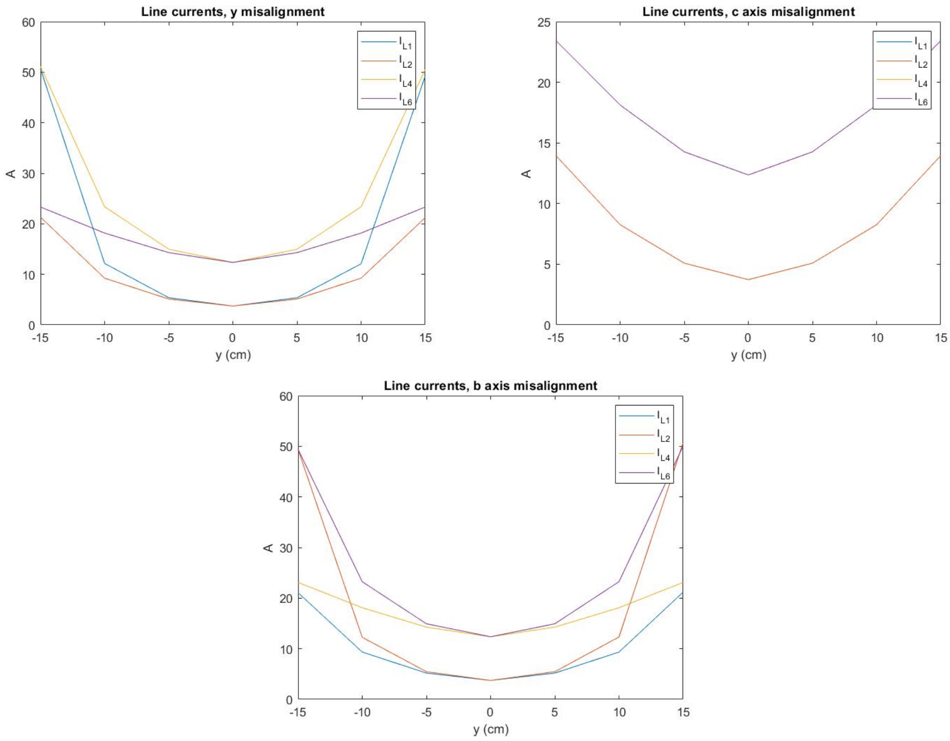

Figure 6.19. Line currents on Tx and Rx-side for misalignments along the three symmetry axes

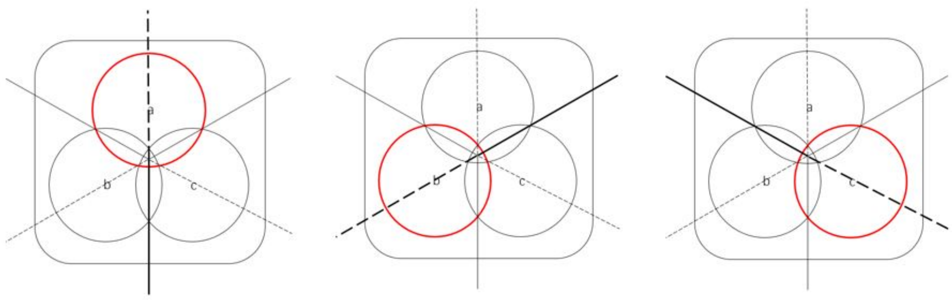

Figure 6.20. Variation of the axis (in black) where null coil current is experienced, changing the non-fed coil (in red)

Knowing the currents of the homologous coils, in case of vertical misalignment between the two pads of the system, it is possible to discriminate between the two possible directions of misalignment.
The real difficulty, however, is to exploit the results just found in practice: as already mentioned in the introduction to the chapter, the currents within the pads are in fact difficult to measure in practice, so a method to recognize the position obtained by means of them is only theoretically possible.
Since misalignment in the $\vec{y}$ axis is generally considered to be the most common, due to errors in a driver's visual assessment, it is in any case interesting to note that, knowing the modules of the line currents exiting the Rx pad, it becomes simple to implement an 'on-line' correction of the incorrect position of the receiving system; in case of misalignment, in fact, the two measured currents do not have the same modulus, while in the aligned case they are identical, as can be seen in Fig.6.19.

Generic $\vec{x} - \vec{y}$ misalignment

Given the results extrapolated from the previous tests, for misalignments along symmetry axes, same tests were carried out for general misalignments.
Since the purpose of this test is to find methods to recognize the exact area of displacement of the Rx pad, between the two possible, circuit simulations were carried out for misalignments along generic lines passing through the origin of the reference system. As done for the previous cases, the trends of the currents passing through the coils (inner currents) were analyzed.
Being outside the symmetry axes, it is possible to neglect the analysis of line currents: they possess perfectly mirror-image trends with respect to the origin, so they are not useful for the intended purpose.
Fig.6.21 shows the results of the analyses performed: the first chart relates to displacements along $y = x$, the second one along $y = -x$, while the third one analyzes the trends for displacements along the x-axis.

As can be seen, in the first case, the ΔI between the homologous currents Tx-Rx has a different sign depending on whether the point has positive or negative ordinate; in the second case, on the other hand, for displacements with small positive ordinate, the ΔI remains negative, but then becomes positive as the ordinate increases. In case of displacement along the $\vec{x}$ axis instead, the ΔI remains negative in both directions of displacement.

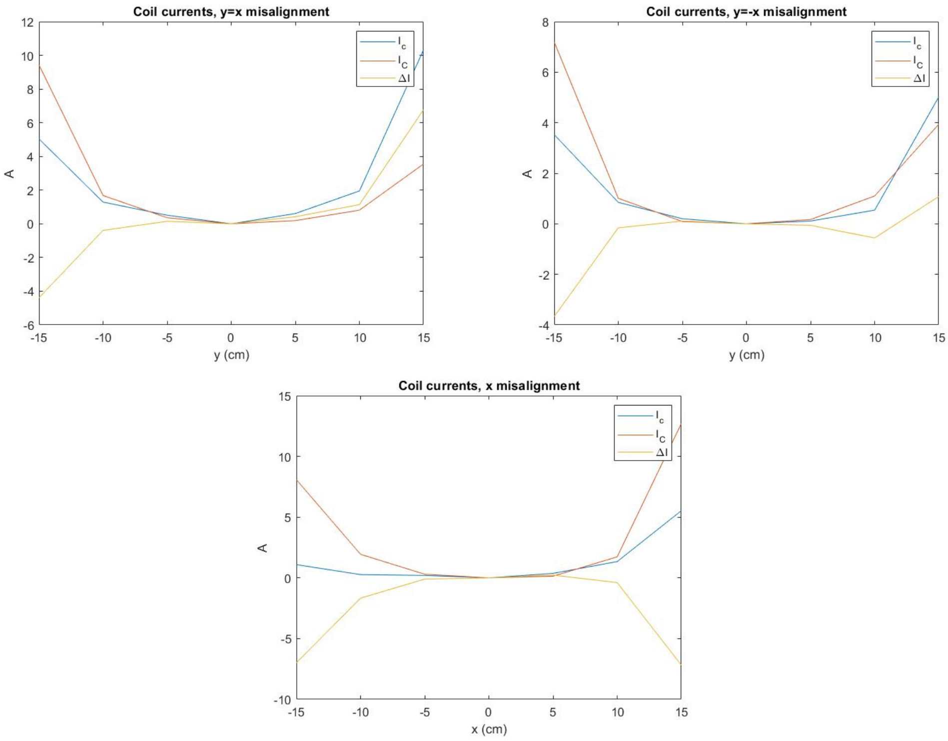

Figure 6.21. Non-fed coil currents for misalignments along $y = x$, $y = -x$ and $y = 0$

Further tests have not allowed to found a general correlation for the identification of the excluded coil currents as the positioning changes. For this reason, an even more detailed analysis of this phenomenon is left to future researches.

Conclusions

Using the magnetic model of the system presented in the first part of this thesis, it was possible to analyze the effects that misalignments of various kinds have on the magnetic and electrical points of view. Symmetries play a key role, as they reduce the complexity of the coupling matrix, which also has an effect on the electrical quantities of the system.
Only in the case of an independent supply of the 6 windings is it possible to unambiguously find the reciprocal position between the two pads, measuring only the output currents magnitudes and phases from the Rx pad.
In the case of delta connection, the coils are not electrically independent, so an analytical solution to the problem is not possible; however, through the tests performed, it was possible to elaborate a map, which for each triplet of line current modules on the Rx side, is able to identify two possible areas of the positioning of the Rx pad, which are mirrored with respect to the axes at the origin.
The power method with opposing phases was therefore designed to uniquely find a displacement area. Although no general solution was found, specific solutions were found in the case of symmetrical misalignments, including one for displacements along the $\vec{y}$ axis. However, these results have limitations from an application point of view, since the data required are the coil currents and not the line ones, which are difficult to be measured.
These results showed that the delta connection, while optimal from an implementation point of view, is not the most convenient for misalignment recognition purposes. In fact, the real advantage of the independent phase system is that the transmitting windings can be supplied independently and their effects on the receiving windings can be studied by decoupling the other Tx-side coils effects.
Possible future studies could focus on new feeding testing procedures so that misalignment can be easily recognized, but also on laboratory experimentation of the tests carried out in the simulations, in order to verify

discrepancies from the simplified model considered, and to make possible modifications.

Bibliography

[1] Emrullah Aydin et al. "Inductive Power Transfer for Electric Vehicle Charging Applications: A Comprehensive Review". In: *Energies 2022, 15, 4962.* (). DOI: DOI:https://doi.org/10.3390/en15144962.

[2] Vincenzo Cirimele et al. "Modelling of a 100 kW-85 kHz three-phase system for static wireless charging and comparison with a classical single-phase system". In: *Department of Energy "G. Ferraris", Politecnico di Torino, Torino, Italy CIRCE-University of Zaragoza, Electrical Engineering Department, Zaragoza, Spain* (2020). DOI: https://doi.org/10.1109/ISCAS45731.2020.9181017.

[3] J. Colussi et al. "100 kW Three-Phase Wireless Charger for EV: Experimental Validation Adopting Opposition Method". In: *Energies 2021, 14, 2113.* (2021). DOI: https://doi.org/10.3390/en14082113.

[4] Jacopo Colussi. "Design and Experimental Validation of a Three-Phase Inductive Power Transfer System Minimizing the Leakage Flux". In: *Doctoral Program in Electrical, Electronic and Communication Enginering (XXXIV cycle)* (2022).

[5] Bryan Esteban et al. "Development of Mutual Inductance Formula for Misaligned Planar Circular Spiral Coils". In: *Department of Electrical and Computer Engineeeing University of Windsor 401 Sunset Avenue Windsor, Ontario* (2015). DOI: https://doi.org/10.1109/ECCE.2015.7309843.

[6] Ahmad Elkhateb Iman Okasili and Timothy Littler. "A Review of Wireless Power Transfer Systems for Electric Vehicle Battery Charging with a Focus on Inductive Coupling". In: *Electronics 2022, 11,*

1355. School of Electronics, Electrical Engineering and Computer Science (EEECS), Queen's University, Belfast (). DOI: DOI:https://doi.org/10.3390/electronics11091355.

[7] Duncan Kon Wui Lo et al. "A Study on Transmission Coil Parameters of Wireless Power Transfer for Electric Vehicles". In: *Serbian Journal of Electrical Engineering Vol. 19, No. 2, June 2022, 129-145* (). DOI: DOI:https://doi.org/10.2298/SJEE2202129L.

[8] Kishore Naik Mude. "Wireless Power Transfer for Electric Vehicle". In: *University of Padova, Italy Department of Industrial Engineering* (CYCLE XXVII°).

[9] Shuang Nie. "Three-phase wireless power transfer for electric vehicle charging with improved receiver misalignment tolerance". In: *Masters of Applied Science Graduate Department of Electrical and Computer Engineering University of Toronto* (2020).

[10] Yuan Song et al. "Three-phase bi-directional wireless EV charging system with high tolerance to pad misalignment". In: *IET Power Electronics, Department of Electrical and Computer Engineering, The University of Auckland, Newmarket, Auckland, New Zealand; School of Electrical Engineering and Computer Science, Queensland University of Technology, Gardens Point Campus, Brisbane, Australia* (2019). DOI: doi:10.1049/iet-pel.2018.6279.